ACS OMEGA

http://pubs.acs.org/journal/acsodf

Article

Mononuclear/Binuclear $[V^{IV}O]/[V^{V}O_2]$ Complexes Derived from 1,3-Diaminoguanidine and Their Catalytic Application for the Oxidation of Benzoin via Oxygen Atom Transfer

Mannar R. Maurya,* Naveen Kumar, and Fernando Avecilla

Cite This: *ACS Omega* 2023, 8, 1301−1318

Read Online

ACCESS | Metrics & More | Article Recommendations | Supporting Information

ABSTRACT: Ligands H_4sal-dag (**I**) and H_4Brsal-dag (**II**) derived from 1,3-diaminoguanidine and salicylaldehyde or 5-bromosalicylaldehyde react with one or 2 mol equivalent of vanadium precursor to give two different series of vanadium complexes. Thus, complexes $[V^{IV}O(H_2sal\text{-}dag)\ (H_2O)]$ (**1**) and $[V^{IV}O(H_2Brsal\text{-}dag)\ (H_2O)]$ (**2**) were isolated by the reaction of an equimolar ratio of these ligands with $[V^{IV}O(acac)_2]$ in MeOH. In the presence of K^+/Cs^+ ion and using aerially oxidized $[V^{IV}O(acac)_2]$, the above reaction gave complexes $[K(H_2O)\{V^{V}O_2(H_2sal\text{-}dag)\}]_2$ (**3**), $[Cs(H_2O)\{V^{V}O_2(H_2sal\text{-}dag)\}]_2$ (**4**), $[K(H_2O)\{VO_2(H_2Brsal\text{-}dag)\}]_2$ (**5**), and $[Cs(H_2O)\text{-}\{V^{V}O_2(H_2Brsal\text{-}dag)\}]_2$ (**6**), which could also be isolated by direct aerial oxidation of complexes **1** and **2** in MeOH in the presence of K^+/Cs^+ ion. Complexes $[(H_2O)V^{IV}O(Hsal\text{-}dag)V^{V}O_2]$ (**7**) and $[(H_2O)V^{IV}O(HBrsal\text{-}dag)V^{V}O_2]$ (**8**) were isolated upon increasing the ligand-to-vanadium precursor molar ratio to 1:2 under an air atmosphere. When **I** and **II** were reacted with aerially oxidized $[V^{IV}O(acac)_2]$ in a 1:2 molar ratio in MeOH in the presence of K^+/Cs^+ ion, they formed $[K(H_2O)_5\{(V^{V}O_2)_2(Hsal\text{-}dag)\}]_2$ (**9**), $[Cs(H_2O)_2\{(V^{V}O_2)_2(Hsal\text{-}dag)\}]_2$ (**10**), $[K_2(H_2O)_4\{(V^{V}O_2)_2(Brsal\text{-}dag)\}]_2$ (**11**), and $[Cs_2(H_2O)_4\{(V^{V}O_2)_2(Brsal\text{-}dag)\}]_2$ (**12**). The structures of complexes **3**, **4**, **5**, and **9** determined by single-crystal X-ray diffraction study confirm the mono-, bi-, tri-, and tetra-anionic behaviors of the ligands. All complexes were found to be an effective catalyst for the oxidation of benzoin to benzil via oxygen atom transfer (OAT) between DMSO and benzoin. Under aerobic condition, this oxidation also proceeds effectively in the absence of DMSO. Electron paramagnetic resonance and ^{51}V NMR studies demonstrated the active role of a stable V(IV) intermediate during OAT between DMSO and benzoin.

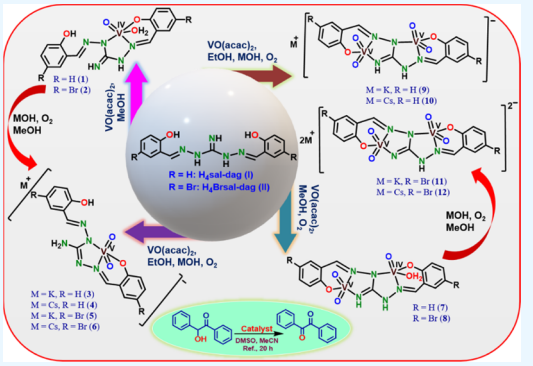

INTRODUCTION

Robenzidene, popularly known as "*Robenidine*," is 1,3-diaminoguanidine-derived N′, 2-bis(€-4-chlorobenzylidene)-hydrazine-1-carboximidhydrazide hydrochloride and was possibly the first compound developed as a poultry anticoccidial agent in the early 1970s. This was later extended to the whole range of apicomplexan parasites causing the disease coccidiosis in other smaller cattle such as dog, cat, sheep, goat, and so forth.[1−7] Very recently, Krollenbrock et al. have prepared *Robenidine* analogues having different substituents on the benzaldehyde moiety and tested them as potential antimalarial drugs in vitro as well as in vivo against *Plasmodium falciparum*, including multidrug-resistant strains.[8] Over the years, modified *Robenidine* analogues have also been prepared by several groups and screened for anti-inflammatory activities.[9] Other areas where such compounds find applications are colorimetric determination of fluoride,[10] chemo sensor for Hg(II) ions,[11] fluorescent detection of Zn(II) ions,[11] and fluorometric determination of microgram level of gallium in biological tissues.[12]

However, the first report on the metal complexes of 1,3-diaminoguanidine-derived ligand (R = H, Scheme 1) appeared in 2008 where binuclear complexes of Cu(II), Ni(II), Mn(II), and V(IV) were isolated, but the structure of only the Cu(II) complex was confirmed by the single-crystal X-ray study (SC-XRD); structures of others were ventured only on the basis of the corresponding (thio)carbohydrazide-derived ligands.[13] Tang et al. reported Ru(II) complexes of ligands presented in Scheme 1 (R = H, 5-Cl, 3,5-Br_2) where ligands were coordinated to Ru(II) as monoanionic NN bidentate, leaving azomethine nitrogens and hydroxyl groups free from coordination.[14] Mononuclear *cis*-$[Mo^{VI}O_2]$ as well as binuclear bis{*cis*-$[Mo^{VI}O_2]$} complexes of the ligand with R = 2,4-di-^{tert}Bu of Scheme 1 were isolated in 2020, and their structures

Received: October 20, 2022
Accepted: December 6, 2022
Published: December 16, 2022

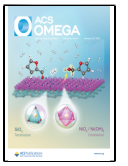

Scheme 1. 1,3-Diaminoguanidine Derived Ligands (I and II) Used in This Study and Ligand III Earlier Used for Vanadium Complexes

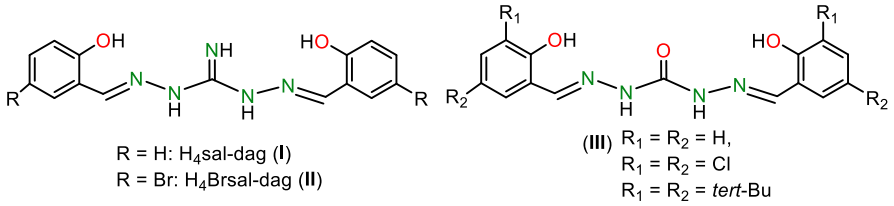

were confirmed by SC-XRD and examined for catalytic potential toward epoxidation of cyclohexene.[15]

Among various transition metals, the coordination chemistry of vanadium has been inspired by its role in biological systems.[16] The presence of vanadate moiety at the active sites of haloperoxidase enzymes and its ability to catalyze oxidation and oxidative bromination of organic molecules by hydrogen peroxide[17] attracted the attention of researchers to search for its structural as well as functional models.[18,19] In addition to the functional model, vanadium complexes have extensively been explored in other catalytic reactions[20] as well, like peroxidase mimicking,[21] sulphoxidation,[22] bromination,[23] oxidation of alkanes,[24] cyclohexane,[25] phenols and alcohols,[26] oxidative coupling of arenols,[27] epoxidation of olefins,[26c,28] hydroxylation of aromatic hydrocarbons,[28] multicomponent reactions,[29] and so forth.

Since ligands **I** and **II** (Scheme 1) derived from 1,3-diaminoguanidine undergo several tautomeric structures, they show very flexible coordination behaviors. In fact, monobasic ÑN bidentate,[14] tribasic hexadentate,[13] and tetrabasic hexadentate[15] behaviors of these ligands are well established. In principle, these ligands have five titrable protons, but so far only four of them have been found to be deprotonable in metal complexes;[15] therefore, we have also considered them as tetrabasic hexadentate in our study. Thus, compared to vanadium complexes of closely related ligands, 1,5-bis-(substituted 2-hydroxybenzaldehyde)carbohydrazone (**III**),[30,31] where these ligands are restricted to provide two different *ONN* and *ONO* binding sites in a combined triply deprotonated form, ligands **I** and **II**, with flexible coordination behaviors, may present different vanadium coordination chemistries. Our interest in vanadium complexes of polynucleating ligands[19] prompted us to consider ligands **I** and **II** and undertake systematic investigation on their coordination behavior toward vanadium precursor(s). We report herein the isolation of various mononuclear/binuclear $[V^{IV}O]/[V^{V}O_2]$ complexes of **I** and **II** and their characterization and reactivity. It is expected that the electronegative character of the N-donor atom (of amine residue) of one pocket of these ligands may help in recognizing individual vanadium centers by nuclear magnetic resonance (NMR) (^{1}H and ^{51}V) study if unsymmetry exists in binuclear complexes.

Further, benzil is an important substrate in the classic benzil-benzilic rearrangement for the synthesis of biologically active compounds A-Norpreganes.[32] Benzil has also been used as a starting material for the synthesis of important heterocyclic compounds.[33−35] A number of methods are reported in the literature for the oxidation of α-hydroxycarbonyl compounds using different metal-based catalysts including Mn[36] and Cr.[37] However, these methods involve the formation of environmentally toxic and hazardous side products. Noble metal catalysts including ruthenium, gold, palladium, and platinum have also been reported in the literature.[38−46] However, these noble metal-based catalysts are very expensive, and therefore, it is worth developing non-noble transition-metal-based catalysts like vanadium for effective oxidation of α-hydroxycarbonyl compounds. However, it is to be noted that not all oxidovanadium(IV/V) complexes are nontoxic unless they are verified.[47] There is very limited literature on the aerobic oxidation of α-hydroxycarbonyl compounds including benzoin by oxidovanadium(IV/V) based compounds.[48−51] We have reported that dioxidomolybdenum(VI) complexes catalyzed the oxidation of benzoin to benzil using the oxygen atom transfer (OAT) reaction between benzoin and dimethyl sulfoxide (DMSO).[52] However, such an OAT reaction catalyzed by oxido/dioxido-vanadium(IV/V) complexes has not been explored. Therefore, herein we also focus on the catalytic oxidation of benzoin to benzil using the OAT reaction between benzoin and DMSO under aerobic/inert conditions. Role of the active catalytic intermediate in this OAT reaction has also been identified.

EXPERIMENTAL SECTION

Materials and Methods. Analytical reagent grade salicylaldehyde, acetylacetone, 1,3-diaminoguanidine monohydrochloride, DMSO-d_6 (Sigma-Aldrich, USA), and V_2O_5 (Himedia, India) were used as procured. Other chemicals and solvents used in this study were procured from standard sources. Precursor $[V^{IV}O(acac)_2]$[53] was prepared following the literature method.

All measurements were made after drying the ligands and complexes at 100 °C. The CHN analysis of all complexes were carried out on an elementar model Vario-EL-III element analyzer. Infrared (IR) spectra were recorded with KBr pellets on a Nicolet 1100 FT-IR spectrometer. Electronic spectra of the ligands and complexes were recorded in DMSO on a Shimadzu 2600 UV−vis spectrophotometer. ^{1}H, ^{13}C, and ^{51}V NMR spectra were recorded in DMSO-d_6 on a Jeol 500 MHz spectrometer. The electron paramagnetic resonance (EPR) spectra of the complexes were recorded in DMSO at 100 K on a Bruker Biospin EMXmicro A200-9.5/12/S/W spectrometer. High-performance liquid chromatography (HPLC) was performed on a Shimadzu LC-2010A HT instrument in the low-pressure gradient mode with a flow rate of 0.5 mL min^{-1} and an injection volume of 15 μL.

Synthesis of Ligands. The method reported in the literature[10,13] was used to prepare 1,3-bis(2-hydroxyphenylmethylideneamino)guanidine monohydrochloride (H_4sal-dag·HCl) (**I**), and 1,3-bis(5-bromo-2-hydroxyphenylmethylideneamino)guanidine monohydrochloride (H_4Brsal-dag·HCl) (**II**). Characterization data (^{1}H and ^{13}C NMR) presented in the Supporting Information match well with the literature values.

https://doi.org/10.1021/acsomega.2c06732
ACS Omega 2023, 8, 1301−1318

Synthesis of Complexes. *[$V^{IV}O(H_2$sal-dag) (H_2O)] (**1**).* To a methanolic solution (30 mL) of [$V^{IV}O(acac)_2$] (0.265 g, 1.00 mmol) was added H_4sal-dag (**I**) (0.334 g, 1.00 mmol) as solid with shaking, and the resulting reaction mixture was refluxed for ca. 10 h. The reaction mixture was allowed to cool at ambient temperature where a dark brown solid precipitated out within 24 h. The brown solid was filtered, washed with methanol, and dried under vacuum. Yield: 0.260 g (68.4%). $C_{15}H_{15}N_5O_4V$ (MW = 380.26) calcd C, 47.38; H, 3.98; N, 18.42. Found: C, 47.07; H, 4.12; N, 18.24%. UV−vis (DMSO) [λ_{max}, nm (ε, litre mol^{-1} cm^{-1})]: 648 (0.98×10^{-2}), 400 (4.2×10^2), 336 (1.25×10^3), 276 (1.46×10^3), 258 (1.31×10^3). IR (KBr, ν_{max}/cm^{-1}): 1632, 1606 (C═N), 996 (V═O). ^{1}H NMR (500 MHz, DMSO-d_6): δ/ppm = 11.91 (br, 1H, OH), 10.09 (s, 1H, −C═NH), 9.65 (s, 1H, Ph−CH═N−), 8.70 (s, 1H, Ph−CH═N−), 8.01 (d, 1H, aromatic), 7.65 (s, 2H, aromatic), 7.54 (d, 1H, aromatic), 7.43 (s, 1H, aromatic), 7.25 (s, 1H, aromatic), 6.94 (s, 1H, aromatic), 6.83 (b, 2H, ═CNH).

*[$V^{IV}O(H_2$Brsal-dag) (H_2O)] (**2**).* The brown complex **2** was prepared from [$V^{IV}O(acac)_2$] (0.265 g, 1.00 mmol) and H_4Brsal-dag (**II**) (0.419 g, 1.00 mmol) by adopting the procedure outlined for **1**. Yield = 0.370 g (68.8%). $C_{15}H_{13}Br_2N_5O_4V$ (MW = 538.05) calcd C, 33.48; H, 2.44; N, 13.02. Found: C, 33.92; H, 2.29; N, 13.28%. UV−vis (DMSO) [λ_{max}, nm (ε, litre mol^{-1} cm^{-1})]: 647 (1.23×10^{-2}), 405 (5.85×10^2), 350 (1.26×10^3), 260 (1.79×10^3). IR (KBr, ν_{max}/cm^{-1}): 1639, 1613 (C═N), 970 (V═O). ^{1}H NMR (500 MHz, DMSO-d_6): δ/ppm = 12.05 (br, 1H, OH), 10.32 (s, 1H, −C═NH), 9.51 (s, 1H, Ph−CH═N−), 8.59 (s, 1H, Ph−CH═N−), 8.20 (s, 1H, aromatic), 7.72 (s, 1H, aromatic), 7.62 (s, 1H, aromatic), 7.46 (s, 1H, aromatic), 7.33 (s, 1H, aromatic), 6.85 (s, 1H, aromatic), 6.74 (s, 1H, ═CNH).

*[K(H_2O){$V^{V}O_2$(H_2sal-dag)}]$_2$ (**3**).* A solution of [$V^{IV}O(acac)_2$] (0.265 g, 1.00 mmol) prepared in EtOH (30 mL) was kept open for aerial oxidation at ambient temperature with slow stirring for 2 days. After adding H_4sal-dag (**I**) (0.334 g, 1.00 mmol) as solid, a solution of K_2CO_3 (0.85 g, 1.50 mmol) (prepared in 8 mL EtOH +2 mL H_2O) was added to the reaction mixture. The pH of the resulting reaction mixture was ∼9 after complete addition of potassium carbonate. Thereafter, the reaction mixture was stirred at room temperature for 2 days whereupon a transparent orange-red solution was obtained. The solvent volume was reduced to ca. 10 mL, and the flask was kept at room temperature where an orange-yellow solid precipitated out within 24 h. This was filtered, washed with cold EtOH and dried under vacuum. Keeping the filtrate at room temperature, orange-yellow crystals of **3** suitable for single-crystal X-ray study were formed after ca. 4 days. Yield 0.315 g (71.4%). $C_{30}H_{30}K_2N_{10}O_9V_2$ (MW = 854.71) calcd C, 42.16; H, 3.54; N, 16.39. Found: C, 42.63; H, 3.65; N, 16.68%. UV−vis (DMSO) [λ_{max}, nm (ε, litre mol^{-1} cm^{-1})]: 435 (2.12×10^3), 360 (3.16×10^3), 266 (2.98×10^3). IR (KBr, ν_{max}/cm^{-1}): 1637, 1621 (C═N), 928, 910 (O═V═O). ^{1}H NMR (500 MHz, DMSO-d_6): δ/ppm = 10.75 (br, 1H, OH), 9.16 (s, 1H, Ph−CH═N−), 8.41 (s, 1H, Ph−CH═N−), 7.59 (d, 1H, aromatic), 7.36 (d, 1H, aromatic), 7.20 (t, 1H, aromatic), 7.15 (t, 1H, aromatic), 6.87 (t, 2H, aromatic), 6.69 (m, 2H, aromatic), 5.84 (br, 2H, ═CNH_2).

*[Cs(H_2O){$V^{V}O_2$(H_2sal-dag)}]$_2$ (**4**).* The reddish−orange complex **4** was prepared similarly from [$V^{IV}O(acac)_2$] (0.265 g, 1.00 mmol) and H_4sal-dag (**I**) (0.334 g, 1.00 mmol) in MeOH in the presence of Cs_2CO_3 solution (0.488 g, 1.50 mmol in 8 mL MeOH +2 mL H_2O), as mentioned for **3**. Crystals suitable for single-crystal X-ray study were obtained from the filtrate. Yield 0.360 g (68.1%). $C_{30}H_{30}Cs_2N_{10}O_{10}V_2$ (MW = 1058.32) calcd C, 34.05; H, 2.86; N, 13.24. Found: C, 34.33; H, 2.71; N, 13.03%. UV−vis (DMSO) [λ_{max}, nm (ε, litre mol^{-1} cm^{-1})]: 435 (2.4×10^3), 359 (3.46×10^3), 264 (3.54×10^3). IR (KBr, ν_{max}/cm^{-1}): 1634, 1621 (C═N), 930, 911, 885 (O═V═O). ^{1}H NMR (500 MHz, DMSO-d_6): δ/ppm = 10.74 (s, 1H, OH), 9.15 (s, 1H, Ph−CH═N−), 8.40 (s, 1H, Ph−CH═N−), 7.59 (d, 1H, aromatic), 7.36 (d,1H, aromatic), 7.20 (t, 1H, aromatic), 7.15 (t, 1H, aromatic), 6.86 (m, 2H, aromatic), 6.70 (m, 2H, aromatic) 5.83 (s, 2H, ═CNH_2).

*[K(H_2O){$V^{V}O_2$(H_2Brsal-dag)}]$_2$ (**5**).* Using the procedure outlined for **3**, maroon-red complex **5** was prepared from [$V^{IV}O(acac)_2$] (0.265 g, 1.00 mmol) and H_4Brsal-dag (**II**) (0.419 g, 1.00 mmol) in MeOH in the presence of K_2CO_3 solution (0.85 g, 1.50 mmol in 8 mL MeOH +2 mL H_2O). Crystals suitable for single-crystal X-ray study were obtained from the filtrate. Yield 0.335 g (53.6%). $C_{31}H_{30}Br_4K_2N_{10}O_{11}V_2$ (MW = 1218.34) calcd C, 30.56; H, 2.48; N, 11.50. Found: C, 30.73; H, 2.57; N, 11.28%. UV−vis (DMSO) [λ_{max}, nm (ε, litre mol^{-1} cm^{-1})]: 444 (3.42×10^3), 369 (4.28×10^3), 267 (4.76×10^3). IR (KBr, ν_{max}/cm^{-1}): 1631, 1611 (C═N), 949, 885 (O═V═O). ^{1}H NMR (500 MHz, DMSO-d_6): δ/ppm = 10.47 (br, 1H, OH), 9.08 (s, 1H, Ph−CH═N−), 8.38 (s, 1H, Ph−CH═N−), 7.92 (d, 1H, aromatic), 7.57 (d, 1H, aromatic), 7.27−7.22 (m, 2H, aromatic), 6.83 (d, 1H, aromatic), 6.64 (d, 1H, aromatic), 6.14 (br, 2H, ═CNH_2), 3.37 (br, 2H, coordinated H_2O).

*[Cs(H_2O){$V^{V}O_2$(H_2Brsal-dag)}]$_2$ (**6**).* The yellowish-orange complex **6** was prepared in MeOH taking [$V^{IV}O(acac)_2$] (0.265 g, 1.00 mmol) and H_4Brsal-dag (**II**) (0.419 g, 1.00 mmol) in the presence of Cs_2CO_3 solution (0.488 g, 1.50 mmol in 8 mL EtOH +2 mL H_2O) according to the procedure mentioned for **3**. Yield 0.400 g (58.2%). $C_{30}H_{26}Br_4Cs_2N_{10}O_{10}V_2$ (MW = 1373.91) calcd C, 26.23; H, 1.91; N, 10.20. Found C, 26.42; H, 1.84; N, 10.38%. UV−vis (DMSO) [λ_{max}, nm (ε, litre mol^{-1} cm^{-1})]: 445 (3.26×10^3), 369 (3.72×10^3), 265 (4.5×10^3). IR (KBr, ν_{max}/cm^{-1}): 1643, 1613 (C═N), 917, 864 (O═V═O). ^{1}H NMR (500 MHz, DMSO-d_6): δ/ppm = 10.39 (s, 1H, OH), 9.08 (s, 1H, Ph−CH═N−), 8.38 (s, 1H, Ph−CH═N−), 7.92 (s, 1H, aromatic), 7.57 (s, 1H, aromatic), 7.26 (m, 2H, aromatic), 6.84 (d, 1H, aromatic), 6.63 (d, 1H, aromatic), 6.10 (s, 2H, ═CNH_2).

*[(H_2O)$V^{IV}O$(Hsal-dag)$V^{V}O_2$] (**7**).* Precursor [$V^{IV}O(acac)_2$] (0.663 g, 2.50 mmol) and H_4sal-dag (**I**) (0.334 g, 1.00 mmol) were dissolved together in MeOH (30 mL), and the resulting reaction mixture was refluxed for ca. 10 h. Thereafter, the flask was left open for slow oxidation of the product at room temperature for ca. 2 days with slow stirring where a brown solid precipitated. The solid was filtered, washed with methanol, and dried under vacuum. Yield 0.300 g (64.9%). $C_{15}H_{14}N_5O_6V_2$ (MW = 462.19) calcd C, 38.98; H, 3.05; N, 15.15. Found C, 39.32; H, 2.97; N, 15.28%. UV−vis (DMSO) [λ_{max}, nm (ε, litre mol^{-1} cm^{-1})]: 648 (1.23×10^{-2}), 400 (5.3×10^2), 341 (9.92×10^2), 283 (1.04×10^3), 257 (1.60×10^3). IR (KBr, ν_{max}/cm^{-1}): 1603 (C═N), 961 (V═O), 916, 898 (O═V═O). ^{1}H NMR (500 MHz, DMSO-d_6): δ/ppm = 10.08 (s, 1H, −C═NH), 9.65 (s, 1H, Ph−CH═N−), 8.70 (s, 1H, Ph−CH═N−), 8.31 (s, 2H, Aromatic), 7.65 (s, 1H,

https://doi.org/10.1021/acsomega.2c06732
ACS Omega 2023, 8, 1301−1318

aromatic), 7.52 (s, 1H, aromatic), 7.42 (s, 1H, aromatic), 7.25 (s, 1H, aromatic), 6.84 (b, 3H, aromatic and =CNH).

*$[(H_2O)V^{IV}O(HBrsal\text{-}dag)V^{V}O_2]$ (**8**).* Brown complex **8** was prepared from $[V^{IV}O(acac)_2]$ (0.663 g, 2.50 mmol) and H_4Brsal-dag (**II**) (0.419 g, 1.00 mmol) in MeOH (30 mL) employing the procedure outlined for **7**. Yield 0.390 g (62.9%). $C_{15}H_{12}Br_2N_5O_6V_2$ (MW = 619.98) calcd C, 29.06; H, 1.95; N, 11.30. Found: C, 29.48; H, 1.72; N, 11.43%. UV−vis (DMSO) [λ_{max}, nm (ε, litre mol^{-1} cm^{-1})]: 650 (1.43×10^{-2}), 408 (16.38×10^2), 351 (1.52×10^3), 266 (2.13×10^3). IR (KBr, ν_{max}/cm^{-1}): 1612 (C=N), 955 (V=O), 919, 880 (O=V=O). ^{1}H NMR (paramagnetic) (500 MHz, DMSO-d_6): δ/ppm = 10.37 (br, 1H, −C=NH), 9.58 (s, 1H, Ph−CH=N−), 8.65 (s, 1H, Ph−CH=N−), 8.28 (s, 1H, aromatic), 7.79 (s, 2H, aromatic), 7.51 (s, 1H, aromatic), 6.89 (s, 1H, aromatic), 6.79 (s, 2H, aromatic and =CNH).

*$[K(H_2O)_5\{(V^{V}O_2)_2(Hsal\text{-}dag)\}]_2$ (**9**).* An oxidized solution of $[V^{IV}O(acac)_2]$ (0.663 g, 2.50 mmol) in ethanol (30 mL) was prepared as mentioned for **3**, and to this was added H_4sal-dag (**I**) (0.334 g, 1.00 mmol) as solid followed by KOH solution (0.140 g, 2.50 mmol in 8 mL EtOH +2 mL H_2O) slowly with stirring. This stirring was continued for ca. 3 days where most of the ligand was dissolved and an orange-yellow solution was obtained. This was filtered, and the solvent volume was reduced to half. After keeping the solution overnight, the yellowish-orange solid was precipitated which was filtered, washed with cold EtOH, and dried under vacuum. The filtrate left after slow evaporation gave yellow-orange crystals suitable for single-crystal X-ray study. Combined yield 0.320 g (54.3%). $C_{30}H_{44}K_2N_{10}O_{22}V_4$ (MW = 1178.7) calcd C, 30.57; H, 3.76; N, 11.88. Found: C, 30.82; H, 3.61; N, 12.08%. UV−vis (DMSO) [λ_{max}, nm (ε, litre mol^{-1} cm^{-1})]: 434 (2.64×10^3), 360 (3.8×10^3), 263 (3.98×10^3). IR (KBr, ν_{max}/cm^{-1}): 1609 (C=N), 937, 911, 889 (ν_{sym}O=V=O). ^{1}H NMR (500 MHz, DMSO-d_6): δ/ppm = 11.56 (br, 1H, −C=NH), 9.67 (s, 1H, Ph−CH=N−), 8.62 (s, 1H, Ph−CH=N−), 7.57 (s, 1H, aromatic), 7.50 (d, 1H, aromatic), 7.40 (t, 1H, aromatic), 7.34 (d, 1H, aromatic), 6.90−6.80 (m, 5H, aromatic and =CNH), 3.17 (s, 1H, coordinated H_2O).

*$[Cs(H_2O)_2\{(V^{V}O_2)_2(Hsal\text{-}dag)\}]_2$ (**10**).* Complex **10** was prepared in EtOH from $[V^{IV}O(acac)_2]$ (0.663 g, 2.50 mmol) and H_4sal-dag (**I**) (0.334 g, 1.00 mmol) in the presence of Cs_2CO_3 solution (0.815 g, 2.50 mmol in 8 mL of EtOH +2 mL of H_2O) using the procedure presented for **9**. A yellowish-orange solid precipitate was filtered, washed with cold EtOH, and dried under vacuum. Yield 0.580 g (94.9%). $C_{30}H_{32}Cs_2N_{10}O_{16}V_4$ (MW = 1258.22) calcd C, 28.64; H, 2.56; N, 11.13 Found: C, 28.22; H, 2.71; N, 11.28%. UV−vis (DMSO) [λ_{max}, nm (ε, litre mol^{-1} cm^{-1})]: 463 (4.54×10^2), 370 (2.1×10^3), 280 (2.06×10^3), 258 (4.1×10^3). IR (KBr, ν_{max}/cm^{-1}): 1610 (C=N), 937, 927, 917, 894 (O=V=O). ^{1}H NMR (500 MHz, DMSO-d_6): δ/ppm = 11.55 (s, 1H, −C=NH), 9.67 (s, 1H, Ph−CH=N−), 8.63 (s, 1H, Ph−CH=N−), 7.57 (d, 1H, aromatic), 7.52 (d, 1H, aromatic), 7.42 (t, 1H, aromatic), 7.35 (t, 1H, aromatic), 6.90 (t, 1H, aromatic), 6.84 (t, 4H, aromatic and =CNH).

*$[K_2(H_2O)_4\{(V^{V}O_2)_2(Brsal\text{-}dag)\}]_2$ (**11**).* Orange-yellow complex **11** was prepared in EtOH from $[V^{IV}O(acac)_2]$ (0.663 g, 2.50 mmol) and H_4Brsal-dag (**II**) (0.419 g, 1.00 mmol) in the presence of Cs_2CO_3 solution (0.815 g, 2.50 mmol in 8 mL of EtOH +2 mL of H_2O) using the procedure presented for **9**. Yield 0.390 g (47.4%). $C_{30}H_{34}Br_4K_4N_{10}O_{20}V_4$ (MW = 1534.43) calcd C, 23.48; H, 2.23; N, 9.13. Found: C, 23.72; H, 2.17; N, 9.21%. UV−vis (DMSO) [λ_{max}, nm (ε, litre mol^{-1} cm^{-1})]: 457 (2.86×10^3), 382 (2.94×10^3), 279 (5.5×10^3), 258 (5.52×10^3). IR (KBr, ν_{max}/cm^{-1}): 1616 (C=N), 925, 860 (O=V=O). ^{1}H NMR (500 MHz, DMSO-d_6): δ/ppm = 9.37 (s, 1H, Ph−CH=N−), 8.47 (s, 1H, Ph−CH=N−), 7.65 (s, 1H, aromatic), 7.59 (s, 1H, aromatic), 7.37 (t, 2H, aromatic), 6.74 (d, 2H, aromatic), 6.47 (b, 1H, =CNH), 3.17 (s, 1H, coordinated H_2O).

*$[Cs_2(H_2O)_4\{(V^{V}O_2)_2(Brsal\text{-}dag)\}]_2$ (**12**).* Orange-yellow complex **12** was prepared in EtOH from $[V^{IV}O(acac)_2]$ (0.663 g, 2.50 mmol) and H_4Brsal-dag (**II**) (0.419 g, 1.00 mmol) in the presence of Cs_2CO_3 solution (0.815 g, 2.50 mmol in 8 mL of EtOH +2 mL of H_2O) following the procedure outlines for **9**. Yield 0.772 g (84.0%). $C_{30}H_{34}Br_4Cs_4N_{10}O_{20}V_4$ (MW = 1909.66) calcd C, 18.87; H, 1.79; N, 7.33. Found: C, 19.06; H, 1.66; N, 7.45%. UV−vis (DMSO) [λ_{max}, nm (ε, litre mol^{-1} cm^{-1})]: 458 (4.14×10^3), 382 (3.06×10^3), 298 (4.66×10^3), 257 (5.04×10^3). IR (KBr, ν_{max}/cm^{-1}): 1607 (C=N), 923, 867 (O=V=O). ^{1}H NMR (500 MHz, DMSO-d_6): δ/ppm = 9.10 (s, 1H, Ph−CH=N−), 8.30 (s, 1H, Ph−CH=N−), 7.46 (d, 2H, aromatic), 7.24 (m, 2H, aromatic), 6.67 (m, 2H, aromatic), 5.70 (b, 1H, =CNH).

X-ray Crystal Structure Determination. Three-dimensional X-ray data were collected on a Bruker Kappa Apex CCD diffractometer at 293 K for compounds **3**, **4**, **5**, and **9** by the $\phi-\omega$ scan method. Reflections were measured from a hemisphere of data collected from frames, each of them covering 0.3° in ω. A total of 58215 for **3**, 13654 for **4**, 34841 for **5**, and 11861 for **9** reflections measured were corrected for Lorentz and polarization effects and for absorption by multiscan methods based on symmetry-equivalent and repeated reflections. Of the total, 3841 for **3**, 4120 for **4**, 4921 for **5**, and 4290 for **9** independent reflections exceeded the significance level ($|F|/\sigma|F|$) > 4.0. After data collection, a multiscan absorption correction (SADABS)[54] was applied in each case. The structures of compounds **3**, **4**, and **5** were solved by direct methods and refined by full matrix least-squares on F^2 data using Olex2,[55] and the structure of **9** was solved and refined using SHELX suite of programs.[56] Hydrogen atoms were located in a difference Fourier map and left to refine freely in compound **4**, except for O(5), which was located in a difference Fourier map and fixed to the oxygen atom. In the other three compounds, hydrogen atoms were included in calculated positions and refined in the riding mode, except for C(3), O(4), C(4), C(5), C(7), C(9), C(14), and C(15) in compound **3**, O(1M), C(2), N(3), O(4), C(5), C(11), C(13), and C(14) in compound **5**, and O(3W) and N(5) in compound **9**, which were located in a difference Fourier map and left to refine freely. Refinements were done with allowance for thermal anisotropy of all non-hydrogen atoms. Compound **3** presents a disorder on the oxygen atom of the half-coordinated ethanol molecule and compound **9** on one water molecule. These disorders have been refined, and two atomic sites have been observed and refined for the atoms implied with the anisotropic atomic displacement parameters. More specifically, these disorders were refined using 17 and 12 restraints in compound **3** and compound **9**, respectively (SADI, SIMU, and DELU restraints were used). The site occupancy factors were 0.50738 for O(1SA) in compound **3** and 0.82932 for O(1WA) in compound **9**. In compound **5**, the hydrogen atoms of water molecule present in the crystal packing were not located. A final difference Fourier map showed no residual electronic density: 0.65 and −0.43 e Å^{-3}

https://doi.org/10.1021/acsomega.2c06732
ACS Omega 2023, 8, 1301−1318

Table 1. Crystal Data and Structure Refinement for 3, 4, 5, and 9

	3	4	5	9
formula	$C_{16}H_{17}N_5O_{4.5}KV$	$C_{15}H_{14}N_5O_5VCs$	$C_{16}H_{17}Br_2KN_5O_6V$	$C_{15}H_{22}KN_5O_{11}V_2$
formula weight	441.384	528.156	625.19	589.36
T, K	293(2)	293(2)	293(2)	293(2)
wavelength, Å	0.71073	0.71073	0.71073	0.71073
crystal system	orthorhombic	triclinic	monoclinic	triclinic
space group	*Pbca*	$P\bar{1}$	$P2_1/c$	$P\bar{1}$
a/Å	11.0214(5)	6.9094(4)	8.0685(4)	6.9544(13)
b/Å	14.4994(7)	11.2611(6)	29.1227(15)	11.256(2)
c/Å	25.0218(13)	11.6773(6)	9.5344(5)	15.632(3)
α/deg	90	95.021(1)	90	71.482(6)
β/deg	90	96.263(1)	109.2720(10)	89.174(5)
γ/deg	90	99.426(1)	90	84.835(5)
V/Å^3	3998.6(3)	885.80(8)	2114.81(19)	1155.5(4)
Z	8	2	4	2
F_{000}	1813.0	514.4	1233.0	600
D_{calc}/g cm^{-3}	1.466	1.980	1.964	1.694
μ/mm^{-1}	0.738	2.624	4.489	1.054
2θ/(deg)	4.92 to 56.64	6.02 to 56.72	4.74 to 68.76	6.46 to 56.70
R_{int}	0.0532	0.0546	0.0507	0.0485
crystal size/mm^3	0.30 × 0.20 × 0.10	0.3 × 0.2 × 0.1	0.3 × 0.2 × 0.1	0.21 × 0.16 × 0.08
goodness-of-fit on F^2	1.062	1.051	1.048	1.024
$R_1[I > 2\sigma(I)]$[a]	0.0439	0.0340	0.0426	0.0596
wR_2(all data)[b]	0.1561	0.0842	0.1161	0.1679
largest differences peak and hole (eÅ^{-3})	0.65 and −0.43	1.85 and −1.44	1.87 and −1.47	1.649 and −0.692

[a]$R_1 = \Sigma||F_o| - |F_c||/\Sigma|F_o|$. [b]$wR_2 = \{\Sigma[w(|F_o|^2 - |F_c|^2)^2]/\Sigma[w(F_o^2)^2]\}^{1/2}$.

Scheme 2. Synthetic Routes to Prepare Different Types of Vanadium Complexes[a]

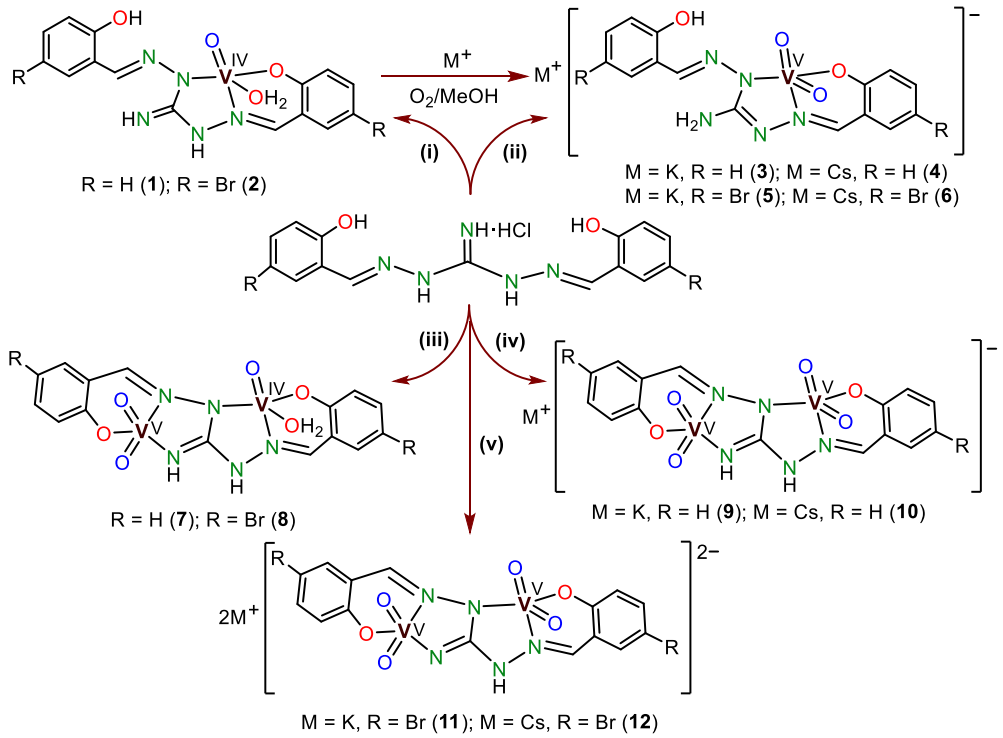

[a](a) Reaction Conditions: (i) [$V^{IV}O(acac)_2$] (M/L = 1:1)/MeOH, Δ, (ii) [$V^{IV}O(acac)_2$] (M/L = 1:1)/MeOH, K_2CO_3 or Cs_2CO_3(1.5 equiv), RT, (iii) [$V^{IV}O(acac)_2$] (M/L = 2.5:1)/MeOH, Δ, O_2/RT, (iv) [$V^{IV}O(acac)_2$] (M/L = 2.5:1)/EtOH, KOH or Cs_2CO_3 (2.5 equiv), RT, and (v) [$V^{IV}O(acac)_2$] (M/L = 2.5:1)/EtOH, KOH or Cs_2CO_3 (2.5 equiv), RT. (b) Structures of the complexes are based on different studies. For complexes **3**−**6** and **9**−**11**, only the anionic part of the structures is shown.

for **3**. For the others, the final difference Fourier map showed a residual electronic density: 1.85 and −1.44 e Å^{-3} for **4**, 1.87 and −1.46 e Å^{-3} for **5**, and 1.651 and −0.688 e Å^{-3} for **9**, next to the metal atoms. Weighting schemes of w = $1/[\sigma^2(F_o^2)$ +

https://doi.org/10.1021/acsomega.2c06732
ACS Omega 2023, 8, 1301−1318

(0.089468 P)^2 + 2.042964 P] for **3**, 1/[$\sigma^2(F_o^2)$ + (0.026258 P)^2 + 2.582623 P] for **4**, 1/[$\sigma^2(F_o^2)$ + (0.055665 P)^2 + 7.259597 P] for **5**, and 1/[$\sigma^2(F_o^2)$ + (0.072100 P)^2 + 2.567600 P] for **9**, where P = ($|F_o|^2$ + 2$|F_c|^2$)/3, were used in the latter stages of refinement. Further details of the crystal structure determination are given in Table 1.

RESULTS AND DISCUSSION

Synthesis of Complexes and Their Stability. Ligands H_4sal-dag (**I**) and H_4Brsal-dag (**II**) (*c.f.*Scheme 1) have competence to react under aerobic/anaerobic conditions with 1 or 2 mol equivalent of the vanadium precursor in the presence or absence of K^+/Cs^+ ion to give 12 different types of complexes (Scheme 2). Thus, the reaction of equimolar ratio of these ligands with [$V^{IV}O(acac)_2$] in MeOH under an inert atmosphere resulted in the formation of complexes [$V^{IV}O$-(H_2sal-dag) (H_2O)] (**1**) and [$V^{IV}O(H_2$Brsal-dag) (H_2O)] (**2**). Increasing this ratio to 1:2 (L/V precursor) in the presence of air, these ligands provide complexes [$(H_2O)V^{IV}O$(Hsal-dag)$V^{V}O_2$] (**7**) and [$(H_2O)V^{IV}O$(HBrsal-dag)$V^{V}O_2$] (**8**), where one of the V ions is oxidized to oxidation state 5 and generate [$V^{V}O_2$] moiety. Direct aerial oxidation of complexes **1** and **2** in the presence of K^+/Cs^+ ion or the reactions of ligands **I** and **II** with aerially oxidized [$V^{IV}O(acac)_2$] in a 1:1 molar ratio in MeOH in the presence of K^+/Cs^+ ion give complexes [$K(H_2O)\{V^{V}O_2(H_2$sal-dag)$\}]_2$ (**3**), [$Cs(H_2O)\{V^{V}O_2(H_2$sal-dag)$\}]_2$ (**4**), [$K(H_2O)\{VO_2(H_2$Brsal-dag)$\}]_2$ (**5**), and [Cs-$(H_2O)\{V^{V}O_2(H_2$Brsal-dag)$\}]_2$ (**6**). Similarly, carrying out the reactions of **I** and **II** with aerially oxidized [$V^{IV}O(acac)_2$] in a 1:2 molar ratio in MeOH in the presence of K^+/Cs^+ ion form [$K(H_2O)_5\{(V^{V}O_2)_2$(Hsal-dag)$\}]_2$ (**9**), [Cs-$(H_2O)_2\{(V^{V}O_2)_2$(Hsal-dag)$\}]_2$ (**10**), [$K_2(H_2O)_4\{(V^{V}O_2)_2$(Brsal-dag)$\}]_2$ (**11**), and [$Cs_2(H_2O)_4\{(V^{V}O_2)_2$(Brsal-dag)$\}]_2$ (**12**). Whole reaction schemes and structures of different complexes (based on different studies) are summarized in Scheme 2. These complexes were characterized by elemental and thermal analyses, spectroscopic (IR, UV−visible, ^{1}H, ^{13}C, and ^{51}V NMR), and EPR (for [$V^{IV}O$] complexes). Additionally, complexes **3**, **4**, **5**, and **9** were confirmed by single-crystal X-ray diffraction (SC-XRD) study.

All these complexes are stable for a long period at room temperature but show a mass loss corresponding to the coordinated solvent molecule(s) (MeOH, EtOH, and H_2O) over a temperature range of 100−280 °C. All complexes decompose on further heating in two or more exothermic steps with the formation of V_2O_5 and MVO_3 (M^+ = K^+ or Cs^+) at higher temperature (300−800 °C). The observed and calculated values of V_2O_5 and MVO_3 residues are presented in Table S1 [for thermogravimetric analysis (TGA) profiles, see Figure S1], and they confirm the expected composition of complexes.

Structure Descriptions. Figures S2−S5 depict the ORTEP representations of the asymmetric units of the compounds **3**, **4**, **5**, and **9**, respectively. Figures 1−4 show that these compounds form dimeric aggregates; such dimerization has already been observed in other published works.[29] The vanadium metal centers are five-coordinated by two terminal oxygen atoms, which act as bridging with alkali metal ions, and three donor atoms of the ligand, two nitrogen atoms and one oxygen atom. The distances of the vanadium center to the terminal oxygen atoms are similar [V(1)−O(1), 1.6209(19) Å in **3**, 1.649(2) Å in **4** and 1.653(3) Å in **9**;

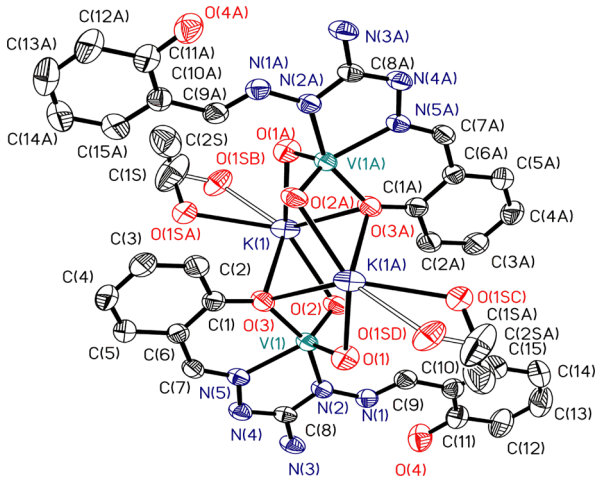

Figure 1. ORTEP of the dimeric aggregate present in the crystal packing of compound **3**, [$K(EtOH)_{0.5}\{VO_2(H_2$sal-dag)$\}]_2$. Non-hydrogen atoms were drawn using 50% probability ellipsoids. Hydrogen atoms are omitted for clarity.

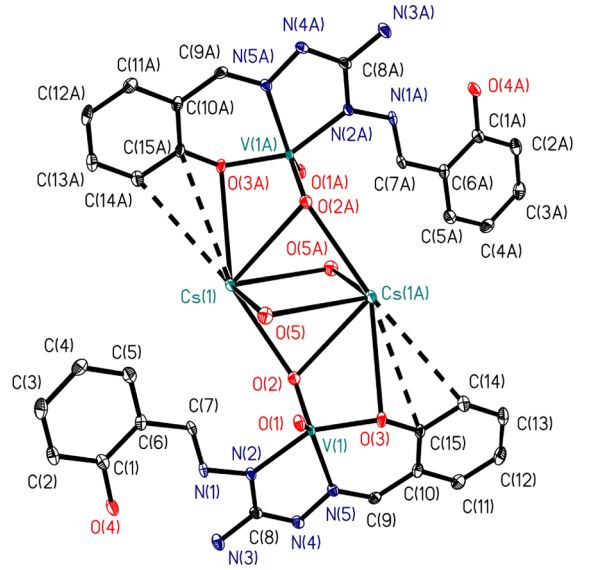

Figure 2. ORTEP of the dimeric aggregate present in the crystal packing of compound **4**, [$Cs(H_2O)\{VO_2(H_2$sal-dag)$\}]_2$. Non-hydrogen atoms were drawn using 50% probability ellipsoids. Hydrogen atoms are omitted for clarity.

V(1)−O(2), 1.6389(18) Å in **3**, 1.632(3) Å in **4**, 1.679(2) Å in **5**, and 1.629(3) Å in **9**], except in the case of the bond length of V(1)−O(1) in compound **5**, which is a little longer, 1.853(2) Å. In **3** and **5**, the oxygen atom of the phenol coordination of the ligand also forms a bridge with the K^+ ion. The distances to water molecules are Cs(1)−O(5), 3.077(3) Å in **4**, K(1)-O(1W), 2.944(6) Å, through the symmetry transformation 1 − *x*, −*y*, 1 − *z*, and 3.420(6) Å and through the symmetry transformation *x* + 1, *y*, and *z* in **5**. The K to water molecules distances are between 2.680(3) and 2.922(14) Å in compound **9**. Table 2 presents the list of the main bond lengths and angles.

The geometric parameter $\tau = (\beta - \alpha)/60$, where β and α are the two largest L−M−L angles, can be used to describe the polyhedron defined by five-coordinated atoms. This parameter has a value of 1 if the structure is pentagonal bipyramidal and 0 if it is square pyramidal. For **3** ($\alpha_{O3-V1-N2}$ = 155.38°,

https://doi.org/10.1021/acsomega.2c06732
ACS Omega 2023, 8, 1301−1318

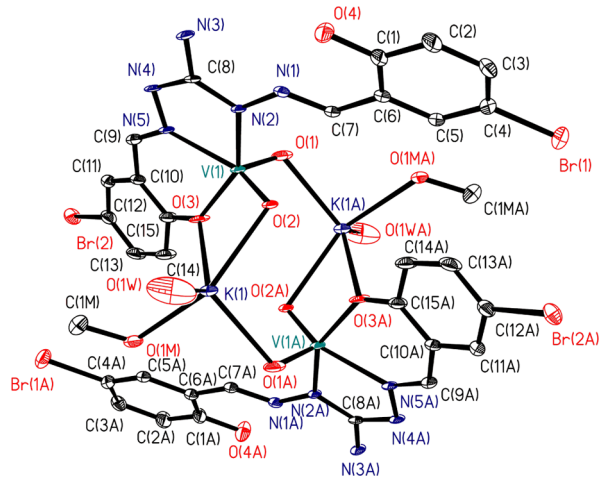

Figure 3. ORTEP of the dimeric aggregate present in the crystal packing of compound **5**, $[K(H_2O)\ (MeOH)\{VO_2(H_2Brsal\text{-}dag)\}]_2$. Non-hydrogen atoms were drawn using 50% probability ellipsoids. Hydrogen atoms are omitted for clarity.

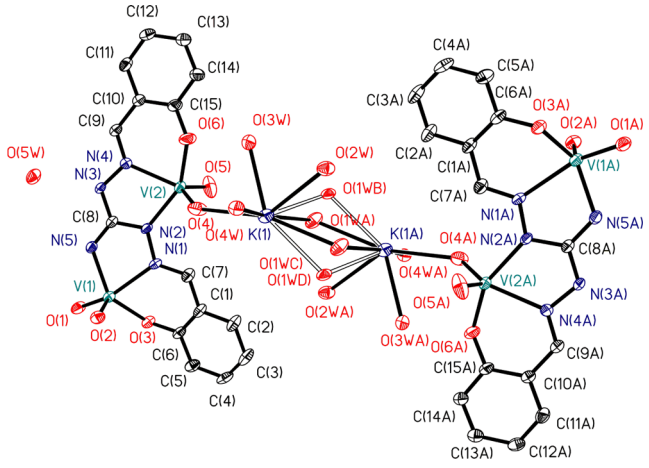

Figure 4. ORTEP of the dimeric aggregate present in the crystal packing of compound **9**, $[K(H_2O)_5\{(V^VO_2)_2(Hsal\text{-}dag)\}]_2$. Non-hydrogen atoms were drawn using 50% probability ellipsoids. Hydrogen atoms are omitted for clarity.

$\beta_{O2-V1-N5}$ = 133.10°), for **4** ($\alpha_{O3-V1-N2}$ = 153.31°, $\beta_{O1-V1-N5}$ = 135.74°), for **5** ($\alpha_{O3-V1-N2}$ = 145.68°, $\beta_{O2-V1-N5}$ = 138.68°), and for **9** [$\alpha_{O1-V1-N1}$ = 153.85°, $\beta_{O3-V1-N5}$ = 138.34°) for V(1) and ($\alpha_{O6-V2-N2}$ = 152.10°, $\beta_{O4-V2-N4}$ = 135.37°) for V(2)], the τ values of 0.37 in **3**, 0.29 in **4**, 0.12 in **5**, and 0.26 for V(1) and 0.27 for V(2) in **9** indicate an intermediate position between the two geometries but closer to that of a square pyramidal polyhedron, especially in the case of compound **5**.[57]

Dimeric aggregate in compound **4** (Figure 2) shows lateral η^2-cation−π interactions of Cs^+ ions and carbon atoms of phenol groups in dashed black lines. The distances to carbon atoms are 3.821(4) Å to C(14) and 3.845(3) Å to C(15). In addition, hydrogen bonds and electrostatic interactions are present in the crystal packing. The ethanol molecule coordinated to the metal center prevents the formation of hydrogen bonds in compound **3**. Table S2 presents the hydrogen bonds that are formed in compounds **4**, **5**, and **9**. Dihedral angles between the phenyl rings [C(1)-C(2)-C(3)-C(4)-C(5)-C(6) and C(10)-C(11)-C(12)-C(13)-C(14)-C(15)], 10.50(16)° in compound **3**, 15.58(6)° in **4**, 38.22(13)° in **5**, and 16.34(9)° in **9**, show that the ligands are basically flat, except in the case of compound **5**, which has a more distorted structure.

While the interaction of the K^+/Cs^+ cation in present complexes with two vanadium centers of two independent molecules of the complex forces these complexes to exit as dimer (**3** and **4**) or tetramer (dimers of dimes; **5** and **9**), binuclear complex of ligand **III**, where NH_4^+ is the counterion, does not facilitate such dimerization because NH_4^+ cation cannot bring such two molecules together through the interaction. However, clustering in two anions occurs through weak interaction of the two sets of oxido groups on different V of one anion with two V of the second one. In other binuclear complexes of **III**, such clustering of two molecules (i.e., dimer of dimer) occurs through two V-(μ-O)-V bridges.[30,31]

IR and UV−Visible Spectral Studies. Three main IR peaks at 3000−3450, 2900−3250, and 1651−1676 cm^{-1} of ligands are worth to consider which are due to ν(O−H), ν(NH), and ν(C═N) stretches, respectively. In binuclear complexes **7**−**12**, there is a sharp band at 1603−1616 cm^{-1}, while in mononuclear complexes, there are at least two such bands in the 1611−1643 cm^{-1} region. The electronic current redistribution due to coordination of one of the azomethine nitrogen possibly pushes the azomethine nitrogen to appear at a lower wave number, justifying the coordination of azomethine nitrogen to V. The ν(O−H) and ν(NH) stretching region is a bit complicated in complexes, and no conclusive interpretation could be made for the phenolate O and other nitrogen(s) coordinated to V. The (O═V═O) group of complexes displays two/three bands at 911−949 and 860−917 cm^{-1}. Such two bands for the (O═V═O) group approve the presence of *cis*-$[VO_2]$ structure in these complexes.[19a] More than two bands in the ionic (Cs^+ and K^+ containing) complexes possibly suggest the weak interaction of such oxygen to Cs^+ and K^+ ions, thereby lowering some of these bands. Complexes **1**, **2**, **7**, and **8** exhibit a sharp foot print at 955−996 cm^{-1} due to the ν(V═O) stretch.

Mono- as well as binuclear complexes display one band at 400−458 nm in the visible region due to ligand-to-metal charge-transfer transition arising due to the transfer of electron density from the filled p-orbital of coordinated oxygen atoms to a vacant d-orbital of vanadium. In $[V^{IV}O]$ complexes, the LMCT band was observed at ca. 400 nm (for ligands' spectra see Figure S6). At higher concentration, a weak shoulder band centered around 650 nm has also been observed which is assigned to d−d transition (Figure 5). Further details are presented in Table S3.

EPR Spectral Study. The X-band first derivative EPR spectra of complexes **1**, **2**, **7**, and **8** were recorded in DMSO at 100 K; the EPR spectra of complexes **2** and **8** are presented in Figure 6 (for others see Figure S7). The spin Hamiltonian parameters (Table 3) were calculated for all complexes from the spectra obtained and are well within the range for normal $[V^{IV}O]$ octahedral complexes having O and N coordination.[58] Considering the weak interaction of DMSO to vanadium in these complexes, a *cis*-form (related to axial oxygen and equatorial DMSO) seems to be more reasonable based on the high value of $[A_z]$ (Table 3).[58] In the EPR spectra of mononuclear as well as binuclear $[V^{IV}O]$ complexes, we observed eight lines without any noticeable broadening, and this confirm the presence of V(IV) center in these complexes. EPR patterns of binuclear complexes **7** and **8** further confirm

https://doi.org/10.1021/acsomega.2c06732
ACS Omega 2023, 8, 1301−1318

Table 2. Bond Lengths [Å] and Angles [°] for the Compounds 3, 4, 5, and 9

compounds	3	4	5	9	
			Bond Lengths		
V(1)−O(1)	1.6209(19)	1.649(2)	1.853(2)		1.653(3)
V(1)−O(2)	1.6389(18)	1.632(3)	1.679(2)		1.629(3)
V(1)−O(3)	1.9356(17)	1.932(2)	1.7867(19)		1.891(3)
V(1)−N(2)	2.033(2)	2.025(3)	1.967(2)	V(1)−N(1)	2.213(3)
V(1)−N(5)	2.1339(19)	2.138(3)	2.052(2)		1.999(3)
C(8)−N(2)	1.355(3)	1.369(4)	1.283(3)	V(2)−O(4)	1.614(3)
C(8)−N(3)	1.353(3)	1.361(4)	1.334(3)	V(2)−O(5)	1.621(3)
C(8)−N(4)	1.320(3)	1.315(4)	1.360(4)	V(2)−O(6)	1.922(3)
				V(2)−N(2)	2.058(3)
				V(2)−N(4)	2.179(3)
				N(2)−C(8)	1.339(5)
				N(3)−C(8)	1.342(5)
V(1)−Cs(1)		3.8434(6)		N(5)−C(8)	1.318(5)
V(1)−K(1)	3.6219(7)		3.1975(7)		
			Angles		
O(2)-V(1)-O(1)	107.99(10)	107.23(12)	113.52(10)		107.28(15)
O(3)-V(1)-O(1)	99.87(9)	93.92(11)	93.94(11)		97.83(13)
O(2)-V(1)-O(3)	95.13(8)	101.66(11)	107.80(8)		106.04(14)
O(1)-V(1)-N(2)	98.72(9)	94.13(11)	115.14(9)	O(1)-V(1)-N(1)	153.85(14)
O(2)-V(1)-N(2)	94.33(8)	100.15(12)	78.05(9)	O(2)-V(1)-N(1)	97.93(13)
O(3)-V(1)-N(2)	155.38(8)	153.31(11)	45.68(10)	O(3)-V(1)-N(1)	81.39(12)
O(1)-V(1)-N(5)	118.42(9)	135.74(12)	107.34(10)		92.36(14)
O(2)-V(1)-N(5)	133.10(8)	116.62(12)	138.68(11)		109.19(14)
O(3)-V(1)-N(5)	83.82(7)	83.31(10)	74.46(8)		138.34(13)

that the unpaired electron of the V(IV) center is localized and not mixed with the V(V) center.

^{1}H NMR Study. Experimental section contains ^{1}H NMR spectral data of ligands and complexes recorded in DMSO-d_6; spectra of H_4sal-dag·HCl (**I**), $[K(H_2O)\{V^VO_2(H_2sal\text{-}dag)\}]_2$ (**3**), and $[K(H_2O)_5\{(V^VO_2)_2(Hsal\text{-}dag)\}]_2$(**9**) as a representative is presented in Figure 7 (for others, see Figures S8−S18). The position of the peaks, particularly assigned to NH/OH protons, was confirmed by D_2O exchange (Figure S19−S24). Thus, two protons of the hydrazide residue (=C−NH−) generally appear as a singlet at ca. 8.77 ppm. One of the two nitrogens of the hydrazide residue coordinates to vanadium after losing the proton, and the remaining =C−NH− proton still resonates as a singlet in complexes **1**, **2**, and **7**−**12** but relatively at upfield (6.47−6.84 ppm) possibly due to electronic current readjustment. However, in complexes **3**−**6**, this proton migrates to −C=NH which converts it to −C−NH_2 and appears at ca. 6.00 ppm along with the vanishing of ca. 8.77 ppm signal. It is to be noted that the −C=NH·HCl group in the amine fragment of ligands exhibits a broad singlet at 12.16−12.30 ppm equivalent to two protons which disappears upon D_2O exchange, indicating their acidic character. The proton of −C=NH group, after losing HCl and coordinating to vanadium, appears at ca. 11.55 ppm (e.g., in complexes **9** and **10**), while when it is only free from HCl, it appears at relatively upfield (10.09−10.32 ppm e.g. in **1** and **2**) compared to those of complexes **9** and **10**. Absence of this signal in complexes **11** and **12** hints toward complete deprotonation and tetra basic behavior of ligands to balance the charges of two K^+/Cs^+ ions per molecule (see Figures S13 and S14). Both ligands show a singlet at 10.30 ppm (in **I**) and 10.72 ppm (in **II**) equivalent to two protons due to phenolic OH. Absence of this signal in binuclear complexes (**7**−**12**) is in agreement with the involvement of both phenolic oxygens in coordination with vanadium. However, the existence of a phenolic signal integrating to one proton in **1**−**6** indicates the involvement of only one of the phenolic oxygens in coordination with vanadium after proton replacement. Similarly, the azomethine protons of ligands resonate at 8.38 (s, 2H in **I**) and at 8.57 (s, 2H in **II**), and the appearance of two such resonances of one proton each with considerable shift to down field in complexes **7**−**12** and the downfield shift of at least one resonance in others (i.e., in **1**−**6**) signify that both azomethine nitrogens are coordinated to vanadium in binuclear complexes while at least one azomethine nitrogen in mononuclear complexes.

^{13}C NMR Study. Comparing the ^{13}C NMR spectra of ligands with the corresponding complexes provides useful information. Due to symmetry in the structure of **I** and **II**, the number of ^{13}C signals is relatively less than the total number of carbons, while complexes generally show signals for all carbons (Table S4). Figure 8 reproduces the spectra of H_4sal-dag·HCl (**I**), $[K(H_2O)\{V^VO_2(H_2sal\text{-}dag)\}]_2$ (**3**), and $[K(H_2O)_5\{(V^VO_2)_2(Hsal\text{-}dag)\}]_2$ (**9**). (For other spectra, see Figures S25−S31). Coordination of metal ion to the ligands causes significant downfield shift $\Delta\delta$ = [δ(complex) − δ(ligand)] in the signal of those carbon atoms that are close to the coordination functionalities like phenolate O-atom(s) (i.e., C1/C1′) and two types of nitrogen atoms (i.e., C7/C7′and C8). In the case of mononuclear complexes, signals related to C1′ and C7′ are least affected; therefore, two signals for such carbons with significant difference in their positions are observed in their spectra. In other cases, normally one signal is observed for each set of carbons (C1/C1′or C7/C7′), and if there are two signals, their positions are very close to each other. Peaks due to carbons of phenyl ring also appear at the expected δ values in the spectra of ligands and complexes.

https://doi.org/10.1021/acsomega.2c06732
ACS Omega 2023, 8, 1301−1318

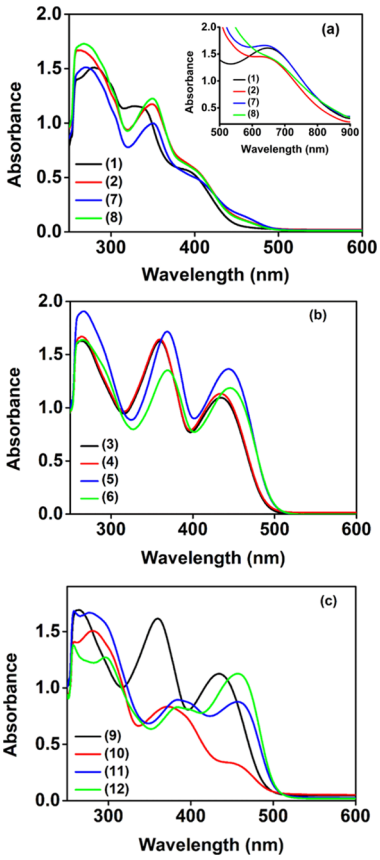

Figure 5. (a) UV−vis spectra of [$V^{IV}O$] complexes recorded in DMSO: **1** (conc. 1.25×10^{-3} M), **2** (conc. 9.29×10^{-4} M), **7** (conc. 1.08×10^{-3} M), and **8** (conc. 8.06×10^{-4} M). Inset shows corresponding spectra in the 500−800 nm range at higher concentration. **1** (conc. 1.64×10^{-2} M), **2** (conc. 1.16×10^{-2} M), **7** (conc. 1.35×10^{-2} M), and **8** (conc. 1.01×10^{-2} M). (b) UV−vis spectra of mononuclear *cis*-[$V^{V}O_2$] complexes recorded in DMSO: **3** (conc. 2.06×10^{-3} M), **4** (conc. 18.90×10^{-4} M), **5** (conc. 16.0×10^{-4} M), and **6** (conc. 14.56×10^{-4} M). (c) UV−vis spectra of binuclear *cis*-[$V^{V}O_2$] complexes recorded in DMSO: **9** (conc. 16.96×10^{-4} M), **10** (conc. 16.36×10^{-4} M), **11** (conc. 12.14×10^{-4} M), and **12** (conc. 10.88×10^{-4} M).

^{51}V NMR Study. The ^{51}V NMR spectra of all *cis*-[$V^{V}O_2$] complexes were measured in DMSO-d_6, and the data are summarized in Table 4. Figure 9 presents the ^{51}V NMR spectra of complexes **3**−**6** and **9**−**12**. The mononuclear complexes show one sharp peak at ca. −447 ppm. On the other hand, binuclear complexes **9**−**11** exhibit two sharp signals of almost

Table 3. Spin Hamiltonian Parameters Obtained from the EPR Spectra of Complexes 1, 2, 7, and 8 Recorded in DMSO at 100 K

compounds	g_x, g_y	$\lvert A_x\rvert$, $\lvert A_y\rvert$ ($\times 10^{-4}$ cm^{-1})	g_z	$\lvert A_z\rvert$ ($\times 10^{-4}$ cm^{-1})
[$V^{IV}O(H_2$sal-dag)(H_2O)] (**1**)	1.991	58.9	1.942	171.9
[$V^{IV}O(H_2$Brsal-dag)(H_2O)] (**2**)	1.992	63.1	1.950	170.2
[(H_2O)$V^{IV}O$(Hsal-dag)$V^{V}O_2$] (**7**)	1.985	67.3	1.947	178.2
[(H_2O)$V^{IV}O$(HBrsal-dag)$V^{V}O_2$] (**8**)	1.993	67.3	1.946	175.4

equal intensity at much upfield that appear at a very narrow range of −559 to −562 and −565 to −572 ppm. A significant upfield shift in binuclear complexes compared to the mononuclear ones is possibly due to more electronegative character of N-donor atoms (of amine residue) relative to O-donor atoms of phenol.[59] While all ^{51}V NMR chemical shifts are consistent with the earlier reported δ_V values for *cis*-[$V^{V}O_2$] complexes,[60] the presence of two signals in binuclear complexes suggests a slight asymmetry in the two vanadium centers even after delocalization of partial electronegative character of N-donor atoms of the amine residue. Accordingly, the signal at the highest upfield region may be assigned to that vanadium which is coordinated to the N-donor atom of the amine residue. These interpretations are also consistent with the crystal structures (vide supra) of particularly mononuclear complexes where coordination functionalities of other than the amine residue site of the ligands are involved in coordination to vanadium. Complex **12**, however, shows only one signal at −559 ppm, showing better symmetry in the two vanadium centers in this complex. Further, the tetrabasic nature of the ligand in **11** and **12** also pushes them to be more symmetric. Thus, when we move from complex **9** to **12** through **10** and **11**, the difference between two signals (in ppm) follows the trend 11(**9**) ≈ 11(**10**) > 6 (**11**) > 0 (**12**), signifying better symmetry in dianionic complexes having a bromo substituent at the ligand.

Reactivity of *cis*-[$V^{V}O_2$] Complexes (3−6 and 9−12) with H_2O_2: a ^{51}V-NMR Study. The reactivity of some selected mono- and binuclear *cis*-[$V^{V}O_2$] complexes with H_2O_2 was also studied by recording the changes in the ^{51}V NMR spectra of these complexes in DMSO-d_6. Addition of 10 equivalents of H_2O_2 to ca. 1.0 mM DMSO-d_6 solution of **4** resulted in no change, while 50 equivalents of H_2O_2 caused the appearance of two additional signals at −561 and −570 ppm

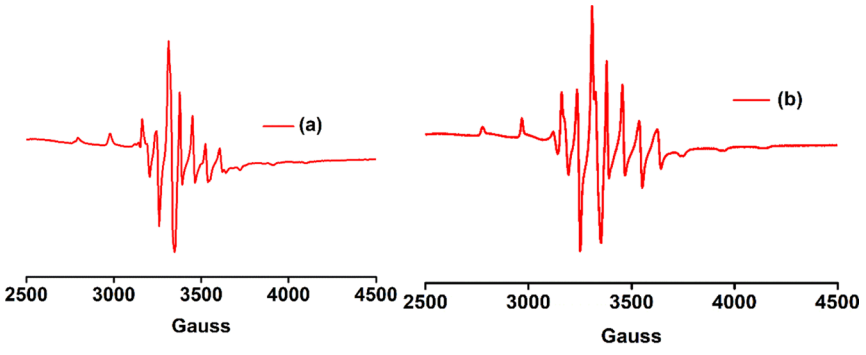

Figure 6. X-band EPR spectrum of **2** (**a**) and **8** (**b**) recorded in DMSO at 100 K.

https://doi.org/10.1021/acsomega.2c06732
ACS Omega 2023, 8, 1301−1318

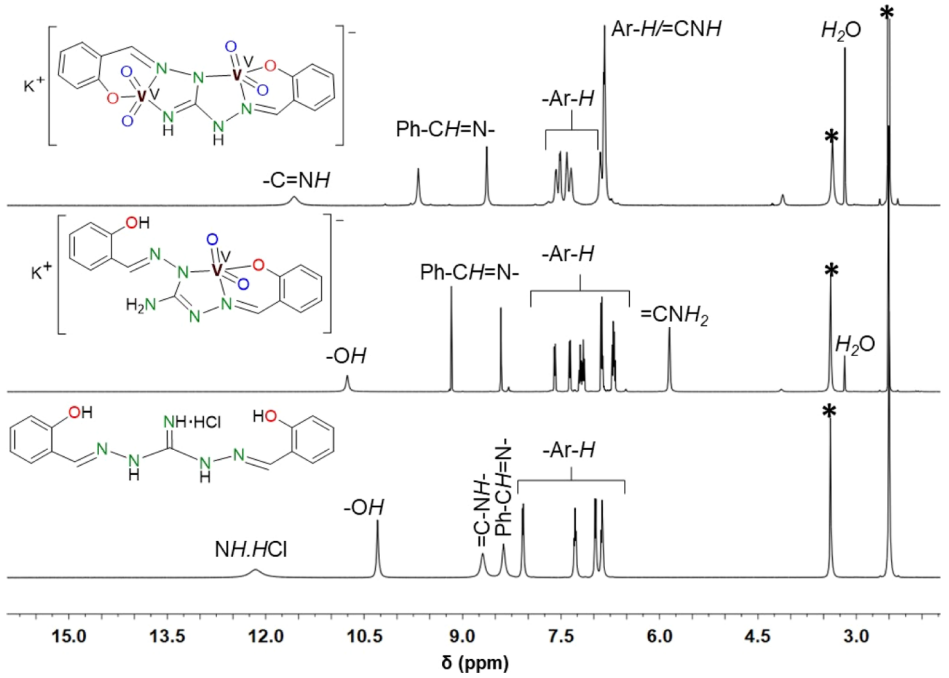

Figure 7. ^{1}H NMR spectra of H_4sal-dag·HCl (**I**), $[K(H_2O)\{V^{V}O_2(H_2sal\text{-}dag)\}]_2$ (**3**), and $[K(H_2O)_5\{(V^{V}O_2)_2(Hsal\text{-}dag)\}]_2$ (**9**). Water in the formula of complexes is not shown for clarity.

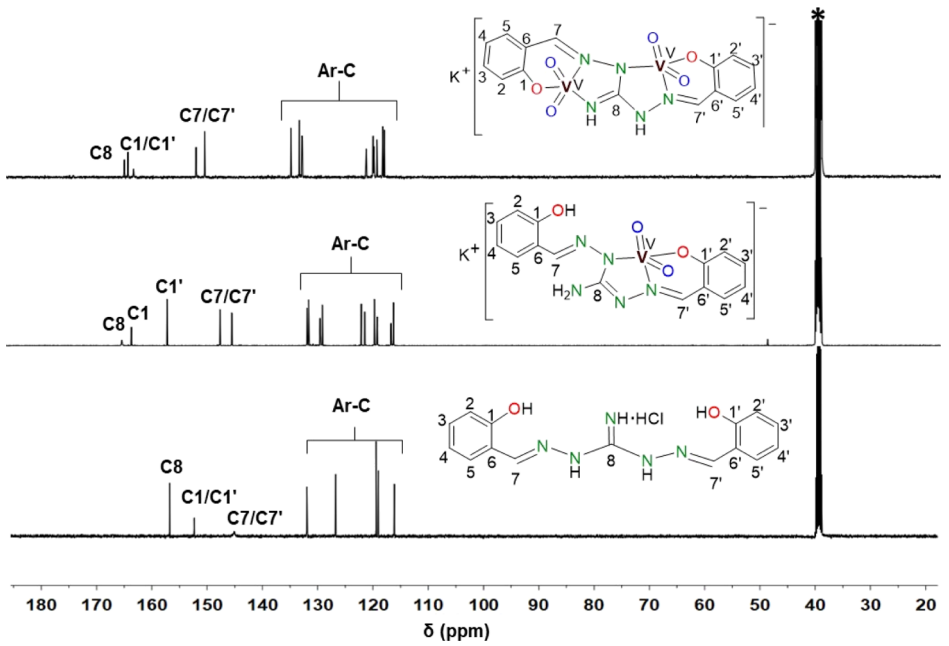

Figure 8. ^{13}C NMR spectra of H_4sal-dag·HCl (**I**) and its vanadium complexes $[K(H_2O)\{V^{V}O_2(H_2sal\text{-}dag)\}]_2$ (**3**) and $[K(H_2O)_5\{(V^{V}O_2)_2(Hsal\text{-}dag)\}]_2$ (**9**).

along with the original one at −547 ppm [Figure 10a]. The additional peaks are well within the range of the peroxidovanadium(V) complexes.[61,62] Almost similar changes were observed for **6** under similar conditions (Figure S32). Similarly, complex **9** does not show any change when 10 equivalents of H_2O_2 was added to it, while addition of 50 equivalents of H_2O_2 resulted in the disappearance of the −561 ppm signal and appearance of one additional signal at −582 ppm. A slight shift in the position of −572 ppm signal to −570 ppm was also noted (Figure 10b). This clearly demonstrates the conversion of one of the dioxido groups to the corresponding oxidoperoxido group. Other binuclear complexes have similar observations (Figures S33 and S34). Interestingly, $[Cs_2(H_2O)_2\{V^{V}O_2\}_2(Brsal\text{-}dag)]_2$ (**12**) under the above conditions (i.e., in the presence of 50 equivalents of H_2O_2) shows two distinct peaks generated at −564 and −576 ppm, while the original −555 ppm peak completely vanished (Figure S35).

The oxidovanadium(IV) complexes **1**, **2**, **7**, and **8** are stable in air as well as in the solvent and therefore are not suitable for direct ^{51}V NMR measurement. Therefore, ^{51}V NMR chemical shift of these complexes was measured after adding different

https://doi.org/10.1021/acsomega.2c06732
ACS Omega 2023, 8, 1301−1318

Table 4. ^{51}V NMR Data of Vanadium Complexes Recorded in DMSO-d_6

sr. no	compound	δ (ppm)	δ (ppm) after addition of H_2O_2
1	$[V^{IV}O(H_2sal\text{-}dag)\ (H_2O)]$ (**1**)		−568, −579
2	$[V^{IV}O(H_2Brsal\text{-}dag)\ (H_2O)]$ (**2**)		−568, −579
3	$[(H_2O)V^{IV}O(Hsal\text{-}dag)V^{V}O_2]$ (**7**)		−567, −578
4	$[[(H_2O)V^{IV}O(HBrsal\text{-}dag)\ V^{V}O_2]$ (**8**)		−568, −579
5	$[K(H_2O)\{V^{V}O_2(H_2sal\text{-}dag)\}]_2$ (**3**)	−548	
6	$[Cs(H_2O)\{V^{V}O_2(H_2sal\text{-}dag)\}]_2$ (**4**)	−547	−547, −561, −570
7	$[K(H_2O)\{VO_2(H_2Brsal\text{-}dag)\}]_2$ (**5**)	−547	
8	$[Cs(H_2O)\{V^{V}O_2(H_2Brsal\text{-}dag)\}]_2$ (**6**)	−547	−547, −561, −570
9	$[K(H_2O)_5\{(V^{V}O_2)_2(Hsal\text{-}dag)\}]_2$ (**9**)	−561, −572	−570, −582
10	$[Cs(H_2O)_2\{(V^{V}O_2)_2(Hsal\text{-}dag)\}]_2$ (**10**)	−562, −573	−570, −582
11	$[K_2(H_2O)_4\{(V^{V}O_2)_2(Brsal\text{-}dag)\}]_2$ (**11**)	−559, −565	−563, −566, −570, −583
12	$[Cs_2(H_2O)_4\{(V^{V}O_2)_2(Brsal\text{-}dag)\}]_2$ (**12**)	−555	−564, −576

amounts of 30% aqueous H_2O_2 to ca. 1.0 mM DMSO-d_6 solutions of these complexes. Thus, no NMR signal could be observed even after adding 20 equivalents of H_2O_2; however, upon addition of 50 equivalents of H_2O_2, these complexes show two peaks in the region −567 to −579 ppm with a major peak at −568 ppm (Figure 11). Compared to the ^{51}V NMR resonance(s) in the corresponding $[V^{V}O_2]$ complexes, these signals are much in upfield, and therefore, we tentatively assign these signals due to the corresponding oxidoperoxidovanadium(V) complexes.[21a,61]

Catalytic Oxidation of Benzoin to Benzil via OAT in the Presence of DMSO. Catalytic oxidation of benzoin was studied considering complex $[K(H_2O)\{V^{V}O_2(H_2sal\text{-}dag)\}]_2$ (**3**) as a representative catalyst (Scheme 3). Initially, various parameters like the amount of complex **3**, the volume of solvent (MeCN), the volume of DMSO, and the temperature of the reaction were optimized for the oxidation of 1.06 g (5 mmol) of benzoin. Finally, for the fixed amount of benzoin, that is, 1.06 g (5 mmol), DMSO (1 mL) and complex **3** (3.0 mg, 3.5×10^{-3} mmol) in 10 mL MeCN were found to be the most ideal ones to carry out the reaction at 80 °C under aerobic condition to get a good yield of benzil. Thus, the decrease in the concentration of benzoin with time was monitored under above reaction conditions aerobically by HPLC using MeCN−water−trifluoroacetic acid mixture (60:40:0.02) as the eluent. The results depicted in Figure 12 show that the conversion of benzoin increases with the elapse of time and reaches 87% along with 100% selectivity toward benzil in 20 h of reaction time.

Catalytic oxidation of benzoin was also performed under an argon atmosphere in the presence as well as absence of DMSO. The obtained conversions are much lower compared to the one carried out under aerobic conditions (49 vs 87% in the presence of DMSO and 41.3 vs 84.6% in the absence) (Table 5). This suggests that complex **3** can also be used as an effective catalyst for the aerobic oxidation of benzoin to benzil. Additionally, this also validates the role of DMSO in the oxidation of benzoin to benzil via OAT as ca. 8% oxidation of benzoin increased in the presence of DMSO. Interestingly, addition of 30% aqueous H_2O_2 does not help in improving the oxidation of benzoin (Table 5, entries 3, 9, and 10). A blank reaction, that is, in the absence of the catalyst, gave only 22% conversion (Table 5, entry 4). Only 3.1% conversion was noted when the reaction was conducted at room temperature under above reaction conditions, while no conversion was observed when the reaction was carried out at room temperature in the absence of the catalyst as well as DMSO.

Keeping in mind the impact of the catalyst and DMSO on the oxidation of benzoin under aerobic condition, catalytic potentials of other vanadium complexes were also checked considering the same mmol of the complexes per metal center, and the results are summarized in Table 6. In general, dioxidovanadium(V) complexes show better activity than oxidovanadium(IV) complexes. However, in spite of lower conversion obtained by oxidovanadium(IV) complexes, the influence of DMSO is much more visible in these complexes

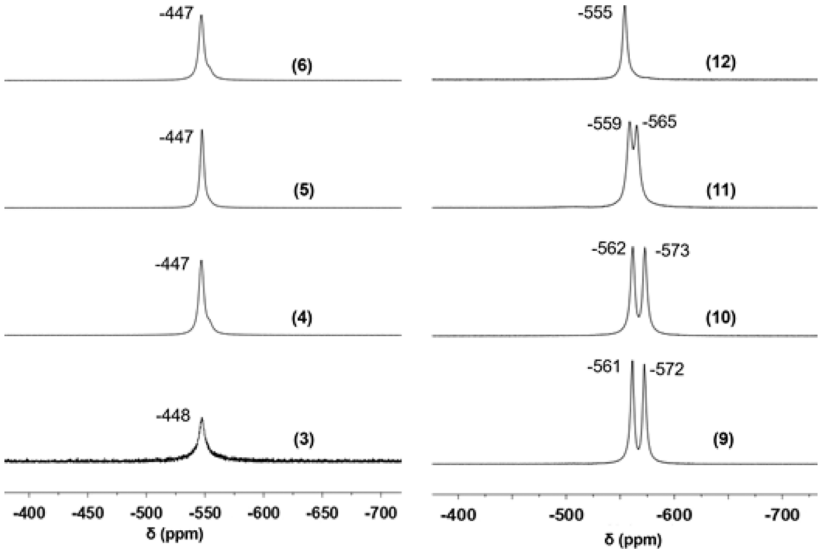

Figure 9. ^{51}V NMR spectra of mononuclear (**3**−**6**) and binuclear *cis*-$[V^{V}O_2]$ complexes (**9**−**12**) recorded in DMSO-d_6.

https://doi.org/10.1021/acsomega.2c06732
ACS Omega 2023, 8, 1301−1318

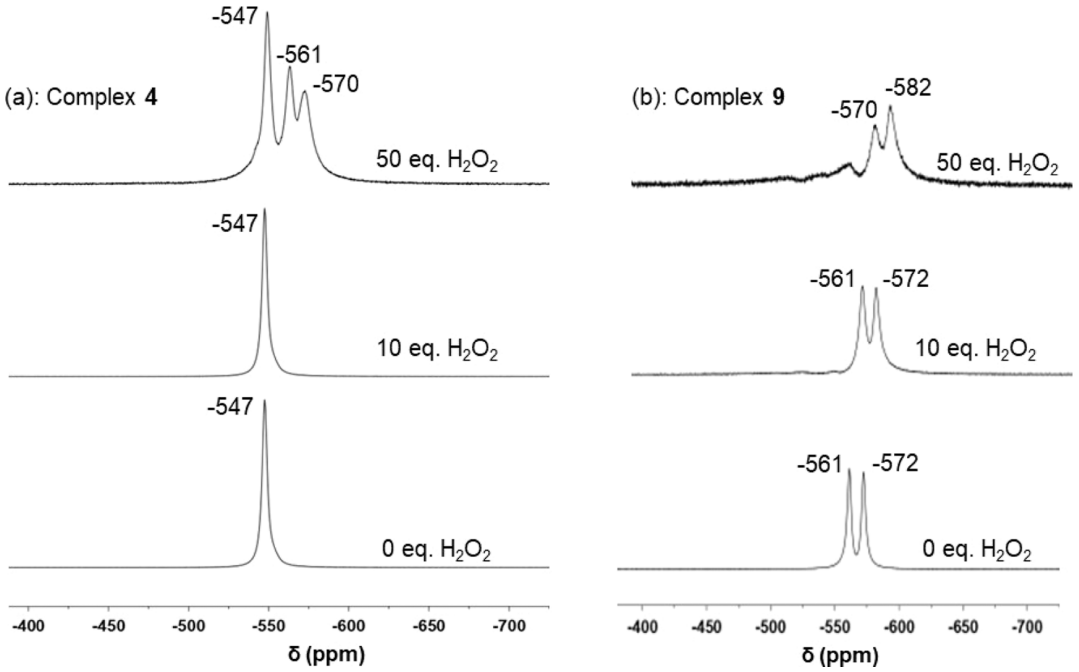

Figure 10. ^{51}V NMR spectra of $[Cs(H_2O)\{V^VO_2(H_2sal\text{-}dag)\}]_2$ (**4**) (a) and $[K(H_2O)_5\{(V^VO_2)_2(Hsal\text{-}dag)\}]_2$(**9**) (b) recorded in DMSO-d_6 and after addition of 30% aq. H_2O_2. Equivalents of H_2O_2 are shown along with the particular spectrum.

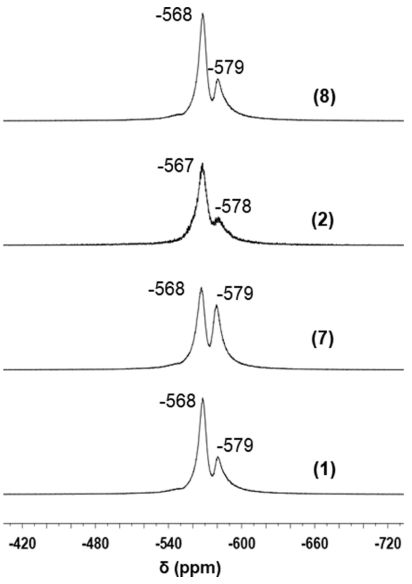

Figure 11. ^{51}V NMR spectra of $[V^{IV}O]$ complexes **1**, **2**, **7**, and **8** recorded in DMSO-d_6 after addition of 50 equivalents of 30% aq. H_2O_2 to ca. 1.0 mM DMSO-d_6 solutions of these complexes.

Scheme 3. Oxidation of Benzoin to Benzil via OAT Catalyzed by Vanadium Complexes

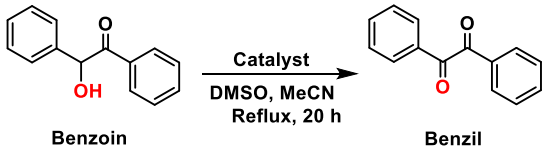

(entry 1 vs 2 of Table 6). Within dioxidovanadium(V) complexes, slightly lower conversion was experienced by the complexes that have bromo bearing on the para position of the benzene ring. Since OAT reaction involves the attack of lone

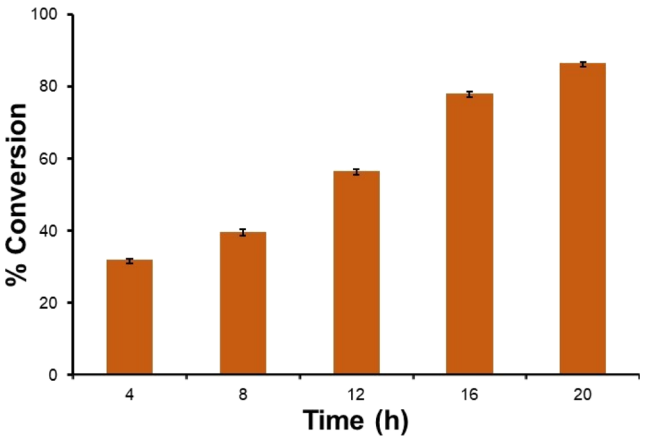

Figure 12. Conversion of benzoin to benzil as a function of time. Reaction conditions: benzoin (1.06 g, 5 mmol), DMSO (1 mL), Catalyst **3** (3.0 mg, 3.5×10^{-3} mmol) and MeCN (10 mL) at 80 °C under aerobic condition. Best of three sets of reactions is considered in each case. The bars also represent the standard deviation of the mean of conversion.

pairs of sulfur on the vanadium center, the presence of the electron-donating group on the benzene ring does not favour such an attack. Though the catalytic system considered here is different from other vanadium complex-catalyzed oxidation of alcohols, these catalysts seem no better than those reported in the literature for the oxidation of alcohols.[26c] A possible reason may be due to their different behaviors in solution.

Mechanistic Study. The role of catalyst in the OAT pathway between DMSO and benzoin is in order by the fact that only 22% conversion of benzoin could be achieved without the complex, while this conversion reached 87% in the presence of catalyst **3**. It follows that DMSO partially oxidizes benzoin to benzil and itself get reduced to dimethyl sulfide. In the presence of catalyst **3** (i.e. *cis*-$[V^VO_2]$ complex), dimethyl sulfide reoxidizes to DMSO and the *cis*-$[V^VO_2]$ species reduces

https://doi.org/10.1021/acsomega.2c06732
ACS Omega 2023, 8, 1301−1318

Table 5. Catalytic Oxidation of Benzoin (1.06 g, 5 mmol) to Benzil Selectively in 20 h of Reaction Time by 3 under Different Reaction Conditions in 10 mL of MeCN

entry no.	catalyst 3 (mg, mmol)	DMSO (mL)	medium	temp (°C)	% conversion of benzoin	TOF (h^{-1})
1	3.0, 3.5×10^{-3}	1	aerobic	80	87	35
2	3.0, 3.5×10^{-3}		aerobic	80	84.6	34
3[a]	3.0, 3.5×10^{-3}	1	aerobic	80	86.5	35
4		1	aerobic	80	22	
5	3.0, 3.5×10^{-3}	1	aerobic	RT	3.1	1
6	3.0, 3.5×10^{-3}		aerobic	RT	no reaction	
7	3.0, 3.5×10^{-3}	1	argon	80	49	20
8	3.0, 3.5×10^{-3}		argon	80	41.3	17
9[a]	3.0, 3.5×10^{-3}		argon	80	17.7	7
10[a]	3.0, 3.5×10^{-3}		aerial	80	27.3	11

[a]Reactions at entries 3, 9, and 10 are in the presence of 30% aqueous H_2O_2 (1.7 g, 15 mmol).

Table 6. Catalytic Oxidation of Benzoin (1.06 g, 5 mmol) to Benzil with 100% Selectivity in 20 h of Reaction Time by Oxido/Dioxido−Vanadium(IV/V) Complexes (1−12)

s. no	catalyst	catalyst[a](mg, mmol)	DMSO (mL)	medium or atmosphere	T (°C)	% conversion	TOF (h^{-1})
1	**1**	2.6, 7.0×10^{-3}	1	aerobic	80	59.4	24
2	**1**	2.6, 7.0×10^{-3}		aerobic	80	25.7	10
3	**2**	3.8, 7.0×10^{-3}	1	aerobic	80	65.7	26
4	**4**	3.7, 3.5×10^{-3}	1	aerobic	80	73.7	30
5	**5**	4.3, 3.5×10^{-3}	1	aerobic	80	56.7	28
6	**6**	4.8, 3.5×10^{-3}	1	aerobic	80	34.7	17
7	**7**	1.6, 3.5×10^{-3}	1	aerobic	80	68.8	55
8	**8**	2.2, 3.5×10^{-3}	1	aerobic	80	70	56
9	**9**	2.1, 1.75×10^{-3}	1	aerobic	80	89.6	72
10	**10**	2.2, 1.75×10^{-3}	1	aerobic	80	69.2	55
11	**11**	2.7, 1.75×10^{-3}	1	aerobic	80	75.8	61
12	**12**	3.4, 1.75×10^{-3}	1	aerobic	80	45.2	36

[a]For all complexes, the catalyst amount is considered per V center.

to a stable [$V^{IV}O$] species in an irreversible manner. This process continues until all dioxidovanadium(V) species is converted to a stable oxidovanadium(IV) species. The oxidovanadium(IV) species further participates in the catalytic cycle, possibly as depicted in Scheme 4. The highly unstable

Scheme 4. Possible Reaction Pathway Involving Oxygen Transfer between Benzoin and DMSO Catalyzed by Oxidovanadium(IV) Complex

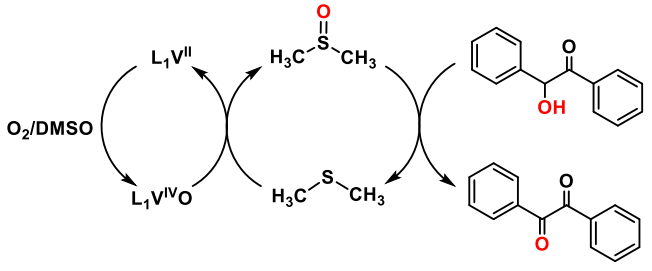

V^{II} species possibly quickly oxidizes to a stable [$V^{IV}O$] in the presence of air/DMSO (see later part of this section). The formation of dimethyl sulfide was confirmed by recording the GC−MS spectrum of the reaction mixture (m/z = 62 for DMS) (Figure S36). Since the reaction takes longer time to acquire equilibrium, the sustainability and stability of the reduced [$V^{IV}O$] species for such a long period were ascertained by monitoring the UV−visible spectral changes of the reaction mixture [i.e., benzoin (5 mmol), DMSO (1 mL), and **3** (10 mg) in 10 mL of MeCN] at 80 °C for ca. 24 h. It is clear from the spectral changes that the reaction starts within a few minutes, but a clear broad band generates at ca. 647 nm due to d−d transition in ca. 6 h of reaction time (Figure 13a. This is further supported by the fact that a sharp peak appearing at −547 ppm in the ^{51}V NMR spectrum [Figure 13b] of complex **3** vanishes after ca. 6 h when a mixture of **3** (4.0 mg), benzoin (100 mg), and DMSO-d_6 (0.6 mL) was heated at 80 °C.

The EPR spectrum of the same reaction mixture (i.e., after 6 h of reaction time at 80 °C) in DMSO at 100 K exhibits eight-line spectrum [Figure 14a] {[g_x, g_y = 1.994, $|A_x|$, $|A_y|$ = 55.9 × 10^{-4} cm^{-1}; g_z = 1.961, $|A_z|$ = 160.4 × 10^{-4} cm^{-1}]}, suggesting the generation of a stable oxidovanadium(IV) species which participates in the catalytic cycle. We have also recorded the EPR spectrum of the same reaction mixture after keeping it at RT for 3 days, and the EPR exhibited a similar eight-line spectrum (Figure S37) confirming the formation of a stable oxovanadium(IV) species, that is, the active species involved in the catalytic cycle. It is to be noted that the EPR spectrum of a reaction mixture containing benzoin (1.06 g, 5 mmol), DMSO (1 mL), acetonitrile (10 mL). and oxidovanadium(IV) complex **1** (5.0 mg) was also recorded after heating the reaction mixture at 80 °C for 6 h, and there was no change in the EPR pattern {[g_x, g_y = 1.993, $|A_x|$, $|A_y|$ = 58.2 × 10^{-4} cm^{-1}], but we were unable to calculate the g_z and $|A_z|$] values because the last resonances at high magnetic field (after 3600−3700 Gauss) are too weak to be observed (Figure 14b), what was obtained with the pure complex **1** in DMSO. However, this

https://doi.org/10.1021/acsomega.2c06732
ACS Omega 2023, 8, 1301−1318

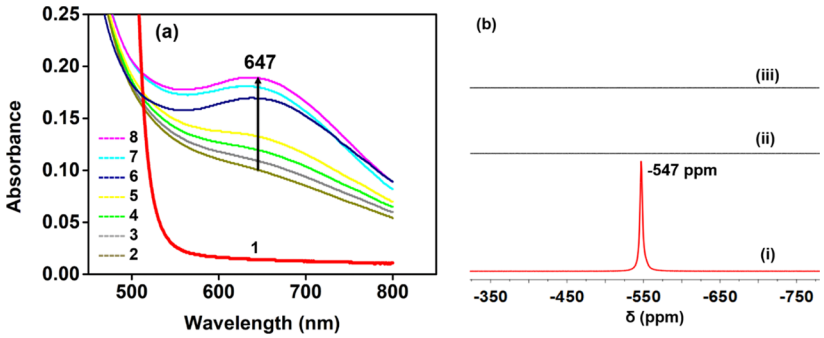

Figure 13. (a) UV−visible spectra of pure catalyst **3** (spectrum 1) and time-dependent spectral changes observed in the OAT reaction between benzoin and DMSO assisted by dioxidovanadium(V) complex **3** in MeCN after 6 h of reaction time: immediately after 6 h at 80 °C (2), after cooling at RT for 30 s (3), after cooling at RT for 60 s (4), after cooling at RT for 5 min (5), after cooling at RT for 6 h (6), after cooling at RT for 16 h (7), and after cooling at RT for 24 h (8). (b) ^{51}V NMR spectra of the reaction containing benzoin (100 mg) and catalyst **3** (5.0 mg) in 0.6 mL of DMSO-d_6: (i) at time zero, (ii) after 6 h of reaction time at 80 °C, and (iii) after keeping the reaction mixture at RT for 24 h.

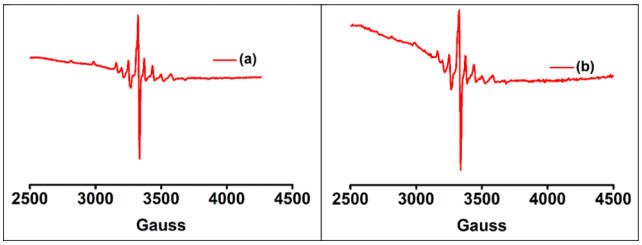

Figure 14. (a) EPR spectrum of the reaction mixture containing benzoin (500 mg), catalyst **3** (4.0 mg), and 1.0 mL of DMSO in 10 mL of MeCN after refluxing the reaction mixture at 80 °C for ca. 6 h. (b) EPR spectrum of the reaction mixture containing benzoin (1.06 g, 5 mmol), complex **1** (5.0 mg), and DMSO (1 mL) in 10 mL of acetonitrile after refluxing the reaction mixture at 80 °C for ca. 6 h. Both spectra were recorded at 100 K.

further stresses the involvement of V(IV) complex in the possible catalytic cycle (Scheme 4).

This mechanism is also supported by the results obtained when the catalytic oxidation of benzoin catalyzed by $V^{IV}O(H_2sal\text{-}dag)$ $(H_2O)]$ (**1**) was performed in the presence and absence of DMSO. The reaction in which DMSO was added gave 59.4% conversion, whereas only 25.7% conversion was achieved when no DMSO was added to the reaction mixture. Thus, DMSO facilitates the oxidation of benzoin to benzil by transferring its oxygen. Running the reaction under aerobic condition further improves the oxidation and thus also approves the role of dioxygen in the catalytic oxidation of benzoin to benzil.

Kinetic Study. We have also studied the kinetics of the decrease of the concentration of benzoin with time for catalysts **1**, **3**, **7**, and **9**. The rate equation (eq 1) for the OAT reaction can be written as

$$\text{rate} = k_{obs}[\text{benzoin}]^x[\text{catalyst}]^y \quad (1)$$

Assuming that the concentration of the catalyst remains largely unaffected during the reaction, eq 1 can be rewritten as eq 2-4.

$$\text{Rate} = k_1[\text{benzoin}]^x \quad (2)$$

where

$$k_1 = k_{obs}[\text{catalyst}]^y \quad (3)$$

$$\ln k_1 = \ln k_{obs} + y \ln[\text{catalyst}] \quad (4)$$

The plot of $1/[\text{benzoin}]_t$ versus time is shown in Figure 15 which suggests that the reaction follows a second-order

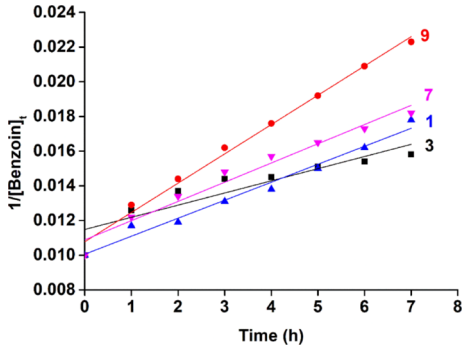

Figure 15. Variation of the concentration of benzoin with time for the oxidation of benzoin to benzil in the presence of DMSO by vanadium complexes (**1**, **3**, **7**, and **9**). Reaction conditions: benzoin (5 mmol. 1.06 g), DMSO (1 mL), MeCN (10 mL), and catalysts **1** (2.6 mg, 7.0×10^{-3} mmol), **3** (3.0 mg, 3.5×10^{-3} mmol), **7** (1.6 mg, 3.5×10^{-3} mmol), and **9** (4.2 mg, 1.75×10^{-3} mmol) at 80 °C.

kinetics with respect to benzoin. The rate equation for a second-order reaction is shown in eq 5.

$$1/[\text{benzoin}]_t = 1/[\text{benzoin}]_o + k_1 t \quad (5)$$

The slope of the line of the plot of $1/[\text{benzoin}]_t$ versus time gave the corresponding rate constants for a second-order reaction (Table 7). Thus, the overall rate equation (eq 5) can be written as

$$\text{rate} = k_{obs}[\text{benzoin}]^2[\text{catalyst}]^y \quad (6)$$

Using the eq 4, the order of the reaction with respect to the catalyst can also be determined by calculating k_1 using different concentrations of, for example, catalyst **3**. The plot of $\ln k_1$ versus ln[catalyst] is shown in Figure 16 and the order of the reaction with respect to the catalyst was found to be 0.72 with $k_{obs} = 3.50 \times 10^{-4}$. Therefore, the overall rate equation for the OAT reaction may be represented as

$$\text{rate} = k_{obs}[\text{benzoin}]^2[\text{catalyst}]^{0.72}$$

$$k_{obs} = 3.50 \times 10^{-4}$$

https://doi.org/10.1021/acsomega.2c06732
ACS Omega 2023, 8, 1301−1318

Table 7. Kinetic Data for the OAT Reaction between Benzoin and DMSO in MeCN at 80 °C under Aerobic Conditions

s. no	catalyst	$K1 \pm SE^a (mol^{-1}\ L\ h^{-1})$	$Kobs \pm SE^a (mol^{-1}\ L\ h^{-1})$
1.	$[V^{IV}O(H_2sal\text{-}dag)\ (H_2O)]$ (1)	$1.04 \times 10^{-4} \pm 1.28 \times 10^{-4}$	
2.	$[K(H_2O)\{V^{V}O_2(H_2sal\text{-}dag)\}]_2$ (3)	$7.01 \times 10^{-4} \pm 6.52 \times 10^{-5}$	$3.50 \times 10^{-4} \pm 6.58\times 10^{-5}$
3.	$[(H_2O)V^{IV}O(Hsal\text{-}dag)V^{V}O_2]$ (7)	$1.11 \times 10^{-4} \pm 5.94 \times 10^{-5}$	
4.	$[K(H_2O)_5\{(V^{V}O_2)_2(Hsal\text{-}dag)\}]_2$ (9)	$1.69 \times 10^{-3} \pm 8.13 \times 10^{-5}$	

[a]Standard error.

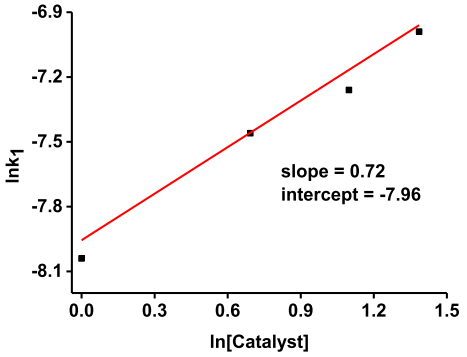

Figure 16. Plot of $\ln k_1$ vs ln[catalyst] for the OAT reaction between benzoin and DMSO catalyzed by **3**.

CONCLUSIONS

In this paper, we have studied the coordination behavior of two polynucleating biaminoguanidine-derived Schiff base ligands H_4sal-dag (**I**) and H_4Brsal-dag (**II**) toward vanadium metal under different reaction conditions. These ligands resulted in complexes $[V^{IV}O(H_2sal\text{-}dag)\ (H_2O)]$ (**1**), $[V^{IV}O(H_2Brsal\text{-}dag)\ (H_2O)]$ (**2**), $[K(H_2O)\{V^{V}O_2(H_2sal\text{-}dag)\}]_2$ (**3**), $[Cs(H_2O)\{V^{V}O_2(H_2sal\text{-}dag)\}]_2$ (**4**), $[K(H_2O)\{VO_2(H_2Brsal\text{-}dag)\}]_2$ (**5**), $[Cs(H_2O)\{V^{V}O_2(H_2Brsal\text{-}dag)\}]_2$ (**6**), $[(H_2O)V^{IV}O(Hsal\text{-}dag)V^{V}O_2]$ (**7**), $[(H_2O)V^{IV}O(HBrsal\text{-}dag)V^{V}O_2]$ (**8**), $[K(H_2O)_5\{(V^{V}O_2)_2(Hsal\text{-}dag)\}]_2$(**9**), $[Cs(H_2O)_2\{(V^{V}O_2)_2(Hsal\text{-}dag)\}]_2$ (**10**), $[K_2(H_2O)_4\{(V^{V}O_2)_2(Brsal\text{-}dag)\}]_2$ (**11**), and $[Cs_2(H_2O)_4\{(V^{V}O_2)_2(Brsal\text{-}dag)\}]_2$ (**12**) which were characterized by various techniques. They behave as dibasic tridentate *ONN* in **1**−**6** where only one vanadium(IV or V) ion is coordinated. In complexes **7** and **8**, these ligands behave as binucleating and accommodate two heterovalent vanadium(IV and V) ions. With the accommodation of two homovalent vanadium(V) ions, these ligands have tribasic $(ONN)_2$ nature in **9** and **10**, while bis(dibasic *ONN*) in **11** and **12**. Interaction of the K^+/Cs^+ cation in complexes with two vanadium centers of two independent molecules of the complex forces **3** and **4** to exit as dimers and **5** and **9** as tetramers (dimers of dimers), but this dimerization is entirely different form the vanadium complexes of ligand **III** reported in the literature[31] However, it is believed that such dimerization should not exist in solution as bond distances associated with the K^+/Cs^+ cation with vanadium are relatively long. Evidenced by NMR and SC-XRD, the coordination functionalities (*ONN*) of the nonamine residue site of the ligands are involved in the coordination to vanadium in mononuclear V(IV) and V(V) complexes. ^{51}V NMR study confirms slight nonsymmetric nature of ligands in **9**−**11**, while **12** is symmetric in nature. The difference between two signals (in ppm) follows the order 11(**9**) ≈ 11(**10**) > 6 (**11**) > 0 (**12**). While all V(IV) complexes give eight-line EPR spectra, the oxidation of V(IV) as well as V(V) complexes, upon reaction with H_2O_2, changes them to the corresponding peroxidovanadium(V) complexes as confirmed by ^{51}V NMR studies. Thus, these ligands behave as mono-, bi-, tri-, and tetra-anionic toward vanadium under different reaction conditions. Such diverse behavior of these ligands is rarely seen in other metal ions.

A limited study has been reported on the catalytic potential of oxidovanadium(IV/V) complexes in the oxidation of benzoin to benzyl and that too under aerobic conditions. The vanadium complexes reported here are effective catalysts for the oxidation of benzoin to benzil via OAT between DMSO and benzoin. Due to the OAT between DMSO and benzoin, the reaction also works under anaerobic conditions. Independent of the catalysts used, a stable oxidovanadium(IV) intermediate is the proposed active species involved in the catalytic cycle which is based on the fact that the intermediate compound shows eight-line EPR spectrum very similar to those exhibited by oxidovanadium(IV) complexes **1**, **2**, **7**, and **8**. This is further supported by the fact that **3** loses its ^{51}V NMR signal during the catalytic reaction and remain ^{51}V NMR silent even after several hours of catalytic reaction. Such identification of the V(IV) catalytic intermediate during the OAT reaction between DMSO and benzoin has not been observed earlier.

ASSOCIATED CONTENT

Supporting Information

The Supporting Information is available free of charge at https://pubs.acs.org/doi/10.1021/acsomega.2c06732.

These data can be obtained free of charge via http://www.ccdc.cam.ac.uk/conts/retrieving.html or from the Cambridge Crystallographic Data Centre, 12 Union Road, Cambridge CB2 1EZ, UK; fax: (+44) 1223 336 033; or e-mail: deposit@ccdc.cam.ac.uk (PDF)

Crystallographic data for **3** (CIF)

Crystallographic data for **4** (CIF)

Crystallographic data for **5** (CIF)

Crystallographic data for **9** (CIF)

AUTHOR INFORMATION

Corresponding Author

Mannar R. Maurya − *Department of Chemistry, Indian Institute of Technology Roorkee, Roorkee 247667, India;* orcid.org/0000-0001-9977-6287; Email: m.maurya@cy.iitr.ac.in

Authors

Naveen Kumar − *Department of Chemistry, Indian Institute of Technology Roorkee, Roorkee 247667, India*

Fernando Avecilla − *Grupo NanoToxGen, Centro de Investigacións Científicas Avanzadas (CICA), Departamento de Química, Facultade de Ciencias, Universidade da Coruña, 15071 A Coruña, Spain*

Complete contact information is available at:

https://doi.org/10.1021/acsomega.2c06732
ACS Omega 2023, 8, 1301−1318

https://pubs.acs.org/10.1021/acsomega.2c06732

Notes

The authors declare no competing financial interest.

■ ACKNOWLEDGMENTS

M.R.M. thanks the Science and Engineering Research Board (SERB), Department of Science and Technology, New Delhi, India for the financial support (grant no. CRG/2018/000182).

■ REFERENCES

(1) Kantor, S.; Kennett, R. L.; Waletzky, E.; Tomcufcik, A. S. 1,3-Bis(p-chlorobenzylideneamino)guanidine hydrochloride (Robenzidene): New poultry anticoccidial agent. *Science* **1970**, *168*, 373−374.
(2) Reid, W. M.; Kowalski, L. M.; Taylor, E. M.; Johnson, J. Efficacy evaluations of robenzidene for control of coccidiosis in chickens. *Avian Dis.* **1970**, *14*, 788−796.
(3) Ryley, J. F.; Wilson, R. G. Studies on the mode of action of the coccidiostat robenidene. *Z. Parasitenkd.* **1971**, *37*, 85−93.
(4) Ryley, J. F.; Wilson, R. G. The development of Eimeria brunetti in tissue culture. *J. Parasitol.* **1972**, *58*, 660−663.
(5) Ryley, J. F.; Wilson, R. G. Comparative studies with anticoccidials and three species of chicken coccidia in vivo and in vitro. *J. Parasitol.* **1972**, *58*, 664−668.
(6) Kennett, R. L.; Kantor, S.; Gallo, A. Efficacy studies with robenidine, a new type of anticoccidial, in the diet. *Poult. Sci.* **1974**, *53*, 978−986.
(7) Wong, D. T.; Horng, J. S.; Wilkinson, J. R. Robenzidene, an inhibitor of oxidative phosphorylation. *Biochem. Biophys. Res. Commun.* **1972**, *46*, 621−627.
(8) Krollenbrock, A.; Li, Y.; Kelly, J. X.; Riscoe, M. K. Robenidine analogues are potent antimalarials in drug-resistant plasmodium falciparum. *ACS Infect. Dis.* **2021**, *7*, 1956−1968.
(9) Sondhi, S. M.; Dinodia, M.; Jain, S.; Kumar, A. Synthesis of biologically active novel bis Schiff bases, bis hydrazine and bis guanidine derivatives. *Indian J. Chem.* **2009**, *48B*, 1129−1136.
(10) Wang, B.; Zhang, P.-Z.; Chen, X.; Jia, A.-Q.; Zhang, Q.-F. Syntheses and crystal structures of guanidine hydrochlorides with two Schiff base functions as efficient colorimetric and selective sensors for fluoride. *Z. Naturforsch.* **2018**, *73*, 601−609.
(11) Rout, K.; Manna, A. K.; Sahu, M.; Patra, G. K. A guanidine based bis Schiff base chemosensor for colorimetric detection of Hg(II) and fluorescent detection of Zn(II) ions. *Inorg. Chim. Acta* **2019**, *486*, 733−741.
(12) Ojeda, C. B.; de Torres, A. G.; Rojas, F. S.; Pavon, J. M. C. Fluorimetric determination of trace amounts of gallium in biological tissues. *Analyst* **1987**, *112*, 1499−1501.
(13) Popov, L. D.; Tupolova, Y. P.; Lukov, V. V.; Shcherbakov, I. N.; Kogan, V. A.; Mishchenko, A. V. Physicochemical study on bis-hydrazone derived from 1,3-diaminoguanidine and salicylaldehyde and its complexes with transition metals. *Russ. J. Gen. Chem.* **2008**, *78*, 2094−2099.
(14) Tang, L. H.; Chen, X.; Jia, A. Q.; Xin, Z.; Zhang, Q. F. Ruthenium(II) complexes of bis-guanidine ligands with substituted Schiff bases. Syntheses and characterization of $[RuH(CO)\{\kappa 2\text{-}N,N\text{-}(2\text{-}HO\text{-}ArCH{=}NN)_2CNH_2\}(PPh_3)_2]$ (Ar = C_6H_4-, 5-Cl-C_6H_3-, 3,5-Br_2-C_6H_2-). *Inorg. Chim. Acta* **2018**, *480*, 108−112.
(15) Jia, A. Q.; Zhou, W. Y.; Wu, S. M.; Shi, H. T.; Zhang, Q. F. Cis-dioxomolybdenum(VI) complexes with diaminoguanidinium and triaminoguanidinium Schiff bases and their catalytic application for epoxidation of cyclohexene. *ChemistrySelect* **2020**, *5*, 11085−11095.
(16) Rehder, D.*Bioinorganic Vanadium Chemistry*; Wiley: Chichester, U.K., 2008.
(17) Butler, A.; Clague, M. J.; Meister, G. E. Vanadium Peroxide Complexes. *Chem. Rev.* **1994**, *94*, 625−638.
(18) (a) Sutradhar, M.; Pombeiro, A. J. L. Coordination chemistry of non-oxido, oxido and dioxidovanadium(IV/V) complexes with azine fragment ligands. *Coord. Chem. Rev.* **2014**, *265*, 89−124. (b) Pessoa, J. C. Thirty years through vanadium chemistry. *J. Inorg. Biochem.* **2015**, *147*, 4−24. (c) Dash, S. P.; Panda, A. K.; Dhaka, S.; Pasayat, S.; Biswas, A.; Maurya, M. R.; Majhi, P. K.; Crochetf, A.; Dinda, R. A study of DNA/BSA interaction and catalytic potential of oxidovanadium(V) complexes with ONO donor ligands. *Dalton Trans.* **2016**, *45*, 18292−18307. (d) Dash, S. P.; Majumder, S.; Banerjee, A.; Carvalho, M. F. N. N.; Adao, P.; Pessoa, J. C.; Brzezinski, K.; Garribba, E.; Reuter, H.; Dinda, R. Chemistry of monomeric and dinuclear non-oxido vanadium(IV) and oxidovanadium(V) aroylazine complexes: Exploring solution behavior. *Inorg. Chem.* **2016**, *55*, 1165−1182. (e) Dash, S. P.; Roy, S.; Mohanty, M.; Carvalho, M. F. N. N.; Kuznetsov, M. L.; Pessoa, J. C.; Kumar, A.; Patil, Y. P.; Crochet, A.; Dinda, R. Versatile reactivity and theoretical evaluation of mono-and dinuclear oxidovanadium(V) compounds of aroylazines: Electrogeneration of mixed-valence divanadium(IV, V) complexes. *Inorg. Chem.* **2016**, *55*, 8407−8421. (f) Roy, S.; Böhme, M.; Dash, S. P.; Mohanty, M.; Buchholz, A.; Plass, W.; Majumder, S.; Kulanthaivel, S.; Banerjee, I.; Reuter, H.; Kaminsky, W.; Dinda, R. Anionic dinuclear oxidovanadium(IV) complexes with azo functionalized tridentate ligands and μ-ethoxido bridge leading to an unsymmetric twisted arrangement: Synthesis, X-ray structure, magnetic properties, and cytotoxicity. *Inorg. Chem.* **2018**, *57*, 5767−5781. (g) Banerjee, A.; Dash, S. P.; Mohanty, M.; Sahu, G.; Sciortino, G.; Garribba, E.; Carvalho, M. F. N. N.; Marques, F.; Pessoa, J. C.; Kaminsky, W.; Brzezinski, K.; Dinda, R. New V^{IV}, $V^{IV}O$, $V^{V}O$, and $V^{V}O_2$ systems: Exploring their interconversion in solution, protein interactions, and cytotoxicity. *Inorg. Chem.* **2020**, *59*, 14042−14057.
(19) (a) Maurya, M. R. Development of the coordination chemistry of vanadium through bis(acetylacetonato)oxovanadium (IV): Synthesis, reactivity and structural aspects. *Coord. Chem. Rev.* **2003**, *237*, 163−181. (b) Maurya, M. R. Probing the synthetic protocols and coordination chemistry of oxido-, dioxido-, oxidoperoxido-vanadium and related complexes of higher nuclearity. *Coord. Chem. Rev.* **2019**, *383*, 43−81. (c) Maurya, M. R.; Kumar, A.; Ebel, M.; Rehder, D. Synthesis, characterization, reactivity and catalytic potential of model vanadium (IV & V) complexes with benzimidazole derived ONN donor ligands. *Inorg. Chem.* **2006**, *45*, 5924−5937. (d) Maurya, M. R.; Khan, A. A.; Azam, A.; Kumar, A.; Ranjan, S.; Mondal, N.; Pessoa, J. C. Dinuclear oxidovanadium(IV) and dioxidovanadium(V) complexes of 5,5'-methylene bis(dibasic tridentate) ligands: Synthesis, spectral characterisation, reactivity, and catalytic and antiamoebic activities. *Eur. J. Inorg. Chem.* **2009**, 5377−5390. (e) Maurya, M. R.; Bisht, M.; Kumar, A.; Kuznetsov, M. L.; Avecilla, F.; Pessoa, J. C. Synthesis, characterization, reactivity and catalytic activity of oxidovanadium(IV), oxidovanadium(V) and dioxidovanadium(V) complexes of benzimidazole modified ligands. *Dalton Trans.* **2011**, *40*, 6968−6983. (f) Maurya, M. R.; Haldar, C.; Kumar, A.; Kuznetsov, M. L.; Avecilla, F.; Pessoa, J. C. Vanadium complexes having $[VO]^{2+}$, $[VO]^{3+}$ and $[VO_2]^{+}$ cores with hydrazones of 2,6-diformyl-4-methylphenol: Synthesis, characterization, reactivity, and catalytic potential. *Dalton Trans.* **2013**, *42*, 11941−11962. (g) Maurya, M. R.; Sarkar, B.; Avecilla, F.; Correia, I. Vanadium(IV and V) complexes derived from acetyl pyrazolone and hydrazides. Structure, reactivity, peroxidase mimic and efficient catalytic activity for the oxidation of 1-phenylethanol. *Eur. J. Inorg. Chem.* **2016**, 4028−4044. (h) Maurya, M. R.; Uprety, B.; Avecilla, F.; Adao, P.; Kuznetsov, M. L.; Pessoa, J. C. Solution behaviour and catalytic potential towards oxidation of dopamine by oxidovanadium(V) complexes of tripodal tetradentate ligands. *Eur. J. Inorg. Chem.* **2017**, 3087−3099. (i) Maurya, M. R.; Jangra, N.; Avecilla, F.; Correia, I. 4,6-Diacetyl resorcinol based vanadium (V) complexes: Reactivity and catalytic applications. *Eur. J. Inorg. Chem.* **2019**, 314−329.
(20) (a) Sutradhar, M.; Martins, L. M. D. R. S.; Silva, M. F. C. G. D.; Pombeiro, A. J. L. Vanadium complexes: Recent progress in oxidation catalysis. *Coord. Chem. Rev.* **2015**, *301*, 200−239. (b) Langeslay, R. R.; Kaphan, D. M.; Marshall, C. L.; Stair, P. C.; Sattelberger, A. P.; Delferro, M. Catalytic applications of vanadium: A mechanistic perspective. *Chem. Rev.* **2019**, *119*, 2128−2191.

https://doi.org/10.1021/acsomega.2c06732
ACS Omega 2023, 8, 1301−1318

(21) (a) Maurya, M. R.; Uprety, B.; Avecilla, F.; Adão, P.; Pessoa, J. C. Vanadium(V) complexes of a tripodal ligand, their characterisation and biological implication. *Dalton Trans.* **2015**, *44*, 17736−17755. (b) Maurya, M. R.; Tomar, R.; Avecilla, F.; Ribeiro, N.; Carvalho, M. F. N. N.; Kuznetsov, M. L.; Correia, I.; Pessoa, J. C. Trinuclear vanadium(IV) and vanadium(V) complexes derived from 2,4,6-triacetylphloroglucinol and study of their peroxidase mimicking activity. *Dalton Trans.* **2020**, *49*, 2589−2609.
(22) Barroso, S.; Adão, P.; Madeira, F.; Duarte, M. T.; Pessoa, J. C.; Martins, A. M. Vanadium diaminebis(phenolate) complexes: Syntheses, structures, and reactivity in sulfoxidation catalysis. *Inorg. Chem.* **2010**, *49*, 7452−7463. (b) Maurya, M. R.; Arya, A.; Kumar, A.; Kuznetsov, M. L.; Avecilla, F.; Pessoa, J. C. Polymer-bound oxidovanadium(IV) and dioxidovanadium(V) complexes as catalysts for the oxidative desulfurization of model fuel diesel. *Inorg. Chem.* **2010**, *49*, 6586−6600.
(23) (a) Maurya, M. R.; Haldar, C.; Khan, A. A.; Azam, A.; Salahuddin, A.; Kumar, A.; Pessoa, J. C. Synthesis, characterization, catalytic and antiamoebic activity of vanadium complexes of binucleating bis(dibasic tridentate ONS donor) ligand systems. *Eur. J. Inorg. Chem.* **2012**, 2560−2577. (b) Maurya, M. R.; Sarkar, B.; Avecilla, F.; Tariq, S.; Azam, A.; Correia, I. Synthesis, characterization, reactivity, catalytic activity, and antiamoebic activity of vanadium(V) complexes of ICL670 (Deferasirox) and a related ligand. *Eur. J. Inorg. Chem.* **2016**, 1430−1441. (c) Maurya, M. R.; Prakash, V.; Avecilla, F.; Sankar, M. Selective bromination of β-positions of porphyrin by self-catalytic behaviour of VOTPP: Facile synthesis, electrochemical redox properties and catalytic application. *Eur. J. Inorg. Chem.* **2021**, 1685−1694. (d) Debnath, M.; Dolai, M.; Pal, K.; Bhunya, S.; Paul, A.; Lee, H. M.; Ali, M. Mono- and dinuclear oxidovanadium(V) complexes of an amine-bis(phenolate) ligand with bromo-peroxidase activities: synthesis, characterization, catalytic, kinetic and computational studies. *Dalton Trans.* **2018**, *47*, 2799−2809.
(24) (a) Sutradhar, M.; Kirillova, M. V.; Guedes da Silva, M. F. C.; Martins, L. M. D. R. S.; Pombeiro, A. J. L. A Hexanuclear mixed-valence oxovanadium(IV, V) complex as a highly efficient alkane oxidation catalyst. *Inorg. Chem.* **2012**, *51*, 11229−11231. (b) Sutradhar, M.; Shvydkiy, N. K.; da Silva, M. F. C. G.; Kirillova, M. V.; Kozlov, Y. N.; Pombeiro, A. J. L.; Shul'pin, G. B. A new binuclear oxovanadium(V) complex as a catalyst in combination with pyrazinecarboxylic acid (PCA) for efficient alkane oxygenation by H2O2. *Dalton Trans.* **2013**, *42*, 11791−11803.
(25) Gupta, S.; Kirillova, M. V.; da Silva, M. F. C. G.; Pombeiro, A. J. L.; Kirillov, A. M. Alkali metal directed assembly of heterometallic VV/M (M = Na, K, Cs) coordination polymers: structures, topological analysis, and oxidation catalytic properties. *Inorg. Chem.* **2013**, *52*, 8601−8611.
(26) (a) Wigington, B. N.; Drummond, M. L.; Cundari, T. R.; Thorn, D. L.; Hanson, S. K.; Scott, S. L. A biomimetic pathway for vanadium-catalyzed aerobic oxidation of alcohols: evidence for a base-assisted dehydrogenation mechanism. *Chem.—Eur. J.* **2012**, *18*, 14981−14988. (b) Maurya, M. R.; Chaudhary, N.; Avecilla, F.; Adão, P.; Pessoa, J. C. Oxidovanadium(IV) and dioxidovanadium(V) complexes of hydrazones of 2-benzoylpyridine and their catalytic applications. *Dalton Trans.* **2015**, *44*, 1211−1232. (c) Maurya, M. R.; Sarkar, B.; Kumar, A.; Ribeiro, N.; Miliute, A.; Pessoa, J. C. New thiosemicarbazide and dithiocarbazate based oxidovanadium(IV) and dioxidovanadium(V) complexes. Reactivity and catalytic potential. *New J. Chem.* **2019**, *43*, 17535−17537.
(27) (27) Sako, M.; Takizawa, S.; Sasai, H. Chiral vanadium complex-catalyzed oxidative coupling of arenols. *Tetrahedron* **2020**, *76*, 131645.
(28) (a) Adão, P.; Pessoa, J. C.; Henriques, R. T.; Kuznetsov, M. L.; Avecilla, F.; Maurya, M. R.; Kumar, U.; Correia, I. Synthesis, characterization, and application of vanadium-salan complexes in oxygen transfer reactions. *Inorg. Chem.* **2009**, *48*, 3542−3561. (b) Maurya, M. R.; Kumar, N. Chloromethylated polystyrene cross-linked with divinylbenzene and grafted with vanadium (IV) and vanadium (V) complexes having ONO donor ligand for the catalytic activity. *J. Mol. Catal. A: Chem.* **2014**, *383*−*384*, 172−181. (c) Maurya, M. R.; Prakash, V.; Avecilla, F.; Sankar, M. Selective epoxidation of olefins by vanadylporphyrin [$V^{IV}O$(TPP)] and electron deficient nonplanar β-octabromovanadyl-porphyrin [$V^{IV}O$(TPPBr8)]. *J. Porph. Phthalocyn.* **2022**, *26*, 187−194.
(29) Maurya, M. R.; Sarkar, B.; Avecilla, F.; Correia, I. Vanadium (IV and V) complexes of pyrazolone based ligands: Synthesis, structural characterization and catalytic application. *Dalton Trans.* **2016**, *45*, 17343−17364.
(30) Hosseini-Monfared, H.; Bikas, R.; Mahboubi-Anarjan, P.; Ng, S. W.; Tiekink, E. R. T. The first neutral dinuclear vanadium complex comprising VO and VO^{2+} cores: synthesis, structure, electrochemical properties, and catalytic activity. *Z. Anorg. Allg. Chem.* **2014**, *640*, 243−248.
(31) Dragancea, D.; Talmaci, N.; Shova, S.; Novitchi, G.; Darvasiova, D.; Rapta, P.; Breza, M.; Galanski, S.; Kozíśek, J.; Martins, N. M. R.; Martins, L. M. D. R. S.; Pombeiro, A. J. L.; Arion, V. B. Vanadium(V) complexes with substituted 1,5-bis(2-hydroxybenzaldehyde)carbohydrazones and their use as catalyst precursors in oxidation of cyclohexane. *Inorg. Chem.* **2016**, *55*, 9187−9203.
(32) Nace, H. R.; Nelander, D. H.; Norsteroids, V. The application of the benzilic acid rearrangement to the synthesis of A-norpregnanes. *J. Org. Chem.* **1964**, *29*, 1677−1681.
(33) Flament, I.; Stoll, M. Pyrazines. 1re communication. I. Synthèse de méthyl-2-pyrazines alcoylées en 3, par condensation de l'éthylènediamine avec les dioxo-2,3-alcanes. *Helv. Chim. Acta* **1967**, *50*, 1754−1758.
(34) Rothkopf, H. W.; Wohrle, D.; Muller, R.; Kossmehl, G. Di- und tetracyanpyrazine. *Chem. Ber.* **1975**, *108*, 875−886.
(35) Wynberg, H.; Kooreman, H. J. The mechanism of the hinsberg thiophene ring synthesis. *J. Am. Chem. Soc.* **1965**, *87*, 1739−1742.
(36) (a) Kamimura, A.; Nozaki, Y.; Nishiyamab, M.; Nakayama, M. Oxidation of benzyl alcohols by semi-stoichiometric amounts of cobalt-doped birnessite-type layered MnO_2 under oxygen atmosphere. *RSC Adv.* **2013**, *3*, 468−472. (b) Taylor, R. J. K.; Reid, M.; Foot, J.; Raw, S. A. Tandem oxidation processes using manganese dioxide: discovery, applications, and current studies. *Acc. Chem. Res.* **2005**, *38*, 851−869.
(37) Luzzio, F. A.; Guziec, F. S. recent applications of oxochromium-amine complexes as oxidants in organic synthesis: a review. *Org. Prep. Proced. Int.* **1988**, *20*, 533−584.
(38) Sarkar, S. K.; Jana, M. S.; Mondal, T. K.; Sinha, C. Alcohol oxidation reactions catalyzed by ruthenium−carbonyl complexes of thioarylazoimidazoles. *Appl. Organomet. Chem.* **2014**, *28*, 641−651.
(39) Liu, H. L.; Liu, Y. L.; Li, Y. W.; Tang, Z. Y.; Jiang, H. F. Metal−organic framework supported gold nanoparticles as a highly active heterogeneous catalyst for aerobic oxidation of alcohols. *J. Phys. Chem. C* **2010**, *114*, 13362−13369.
(40) Rautiainen, S.; Simakova, O.; Guo, H.; Leino, A. R.; Kordas, K.; Murzin, D.; Leskela, M.; Repo, T. Solvent controlled catalysis: Synthesis of aldehyde, acid or ester by selective oxidation of benzyl alcohol with gold nanoparticles on alumina. *Appl. Catal., A* **2014**, *485*, 202−206.
(41) Shang, C.; Liu, Z. P. Origin and activity of gold nanoparticles as aerobic oxidation catalysts in aqueous solution. *J. Am. Chem. Soc.* **2011**, *133*, 9938−9947.
(42) Chen, G. Z.; Wu, S. J.; Liu, H. L.; Jiang, H. F.; Li, Y. W. Palladium supported on an acidic metal−organic framework as an efficient catalyst in selective aerobic oxidation of alcohols. *Green Chem.* **2013**, *15*, 230−235.
(43) Karimi, B.; Khorasani, M.; Vali, H.; Vargas, C.; Luque, R. Palladium nanoparticles supported in the nanospaces of imidazolium-based bifunctional PMOs: The role of plugs in selectivity changeover in aerobic oxidation of alcohols. *ACS Catal.* **2015**, *5*, 4189−4200.
(44) Wang, X.; Wu, G.; Guan, N.; Li, L. Supported Pd catalysts for solvent-free benzyl alcohol selective oxidation: Effects of calcination pretreatments and reconstruction of Pd sites. *Appl. Catal., B* **2012**, *115*, 7−15.

https://doi.org/10.1021/acsomega.2c06732
ACS Omega 2023, 8, 1301−1318

(45) Chen, W.; Xie, Z.; Zheng, H.; Lou, H.; Liu, L. Structurally diverse α-substituted benzopyran synthesis through a practical metal-free C(sp^3)−H functionalization. *Org. Lett.* **2014**, *16*, 5988−5991.
(46) Kaizuka, K.; Miyamura, H.; Kobayashi, S. Remarkable effect of bimetallic nanocluster catalysts for aerobic oxidation of alcohols: Combining metals changes the activities and the reaction pathways to aldehydes/carboxylic acids or esters. *J. Am. Chem. Soc.* **2010**, *132*, 15096−15098.
(47) Assem, F. L.; Levy, L. S. A review of current toxicological concerns on vanadium pentoxide and other vanadium compounds: Gaps in knowledge and directions for future research. *J. Toxicol. Environ. Health, Part B* **2009**, *12*, 289−306.
(48) (a) Kirihara, M.; Ochiai, Y.; Takizawa, S.; Takahata, H.; Nemoto, H. Aerobic oxidation of α-hydroxycarbonyls catalysed by trichlorooxyvanadium: efficient synthesis of α-dicarbonyl compounds. *Chem. Commun.* **1999**, 1387−1388. (b) Radosevich, A. T.; Musich, C.; Toste, F. D. Vanadium-catalyzed asymmetric oxidation of α-hydroxy esters using molecular oxygen as stoichiometric oxidant. *J. Am. Chem. Soc.* **2005**, *127*, 1090−1091.
(49) Chen, C. T.; Kao, J. Q.; Salunke, S. B.; Lin, Y. H. Enantioselective aerobic oxidation of α-hydroxy-ketones catalyzed by oxidovanadium(V) methoxides bearing chiral, N-salicylidene-tert-butylglycinates. *Org. Lett.* **2011**, *13*, 26−29.
(50) Velusamy, S.; Punniyamurthy, T. Novel vanadium-catalyzed oxidation of alcohols to aldehydes and ketones under atmospheric oxygen. *Org. Lett.* **2004**, *6*, 217−219.
(51) Kurbah, S. D.; Asthana, M.; Syiemlieh, I.; Lal, R. A. Peroxidative catalytic oxidation of alcohols catalyzed by hetero-binuclear vanadium(V) complexes using H_2O_2 as terminal oxidizing agents. *Appl. Organomet. Chem.* **2018**, *32*, No. e4299.
(52) Maurya, M. R.; Uprety, B.; Avecilla, F. Dioxidomolybdenum(VI) complexes of tripodal tetradentate ligands for catalytic oxygen atom transfer between benzoin and DMSO and for oxidation of pyrogallol. *Eur. J. Inorg. Chem.* **2016**, *2016*, 4802−4813.
(53) Rowe, R. A.; Jones, M. M. Vanadium(IV)oxy(acetylacetonate). *Inorg. Synth.* **1957**, *5*, 113−116.
(54) Sheldrick, G. M.*SADABS*, version 2.10; University of Göttingen: Germany, 2004.
(55) (a) Dolomanov, O. V.; Bourhis, L. J.; Gildea, R. J.; Howard, J. A. K.; Puschmann, H. OLEX2: A complete structure solution, refinement and analysis program. *J. Appl. Crystallogr.* **2009**, *42*, 339−341. (b) Bourhis, L. J.; Dolomanov, O. V.; Gildea, R. J.; Howard, J. A. K.; Puschmann, H. The anatomy of a comprehensive constrained, restrained refinement program for the modern computing environment − OLEX2 dissected. *Acta Crystallogr.* **2015**, *A71*, 59−75.
(56) Sheldrick, G. M. Crystal structure refinement with SHELXL. *Acta Crystallogr.* **2015**, *C71*, 3−8.
(57) Addison, A. W.; Rao, T. N.; Reedijk, J.; van Rijn, J.; Verschoor, G. C. Synthesis, structure, and spectroscopic properties of copper(II) compounds containing nitrogen-sulphur donor ligands; the crystal and molecular structure of aqua[l,7-bis(N-methylbenzimidazol-2'-yl)-2,6- dithiaheptane]copper(II) Perchlorate. *J. Chem. Soc., Dalton Trans.* **1984**, 1349−1356.
(58) Adão, P.; Maurya, M. R.; Kumar, U.; Avecilla, F.; Henriques, R. T.; Kusnetsov, M. L.; Pessoa, J. C.; Correia, I. Vanadium-salen and -salan complexes: Characterization and application in oxygen transfer reaction. *Pure Appl. Chem.* **2009**, *81*, 1279−1296.
(59) (a) Rehder, D.; Weidemann, C.; Duch, A.; Priebsch, W. 51V Shielding in vanadium(V) complexes: A reference scale for vanadium binding sites in biomolecules. *Inorg. Chem.* **1988**, *27*, 584−587. (b) Priebsch, W.; Rehder, D. Oxovanadium alkoxides: Structure, reactivity and vanadium-51 NMR characteristics. Crystal and molecular structures of tris(2-chloroethoxo)oxovanadium and aquadichlorooxobis(tetrahydrofuran)vanadium. *Inorg. Chem.* **1990**, *29*, 3013−3019.
(60) Pessoa, J. C.; Calhorda, M. J.; Cavaco, I.; Correia, I.; Duarte, M. T.; Felix, V.; Henriques, R. T.; Piedade, M. F. M.; Tomaz, I. Molecular modelling studies of N-salicylideneamino acidato complexes of oxovanadium(IV). Molecular and crystal structure of a new dinuclear LOV^{IV}−O−$V^{V}OL$ mixed valence complex. *J. Chem. Soc., Dalton Trans.* **2002**, 4407−4415.
(61) Conte, V.; Furia, F. D.; More, S. Solvation, preferential solvation and complexation by the solvent of peroxovanadium complexes studied by ^{51}V NMR spectroscopy. Correlations with the oxidative reactivity. *Inorg. Chim. Acta* **1998**, *172*, 62−47.
(62) Slebodnick, C.; Pecoraro, V. L. Solvent effects on ^{51}V NMR chemical shifts: characterization of vanadate and peroxovanadate complexes in mixed water/acetonitrile solvent. *Inorg. Chim. Acta* **1998**, *283*, 37−43.

https://doi.org/10.1021/acsomega.2c06732
ACS Omega 2023, 8, 1301−1318